NASA TN D-1741

55 p.

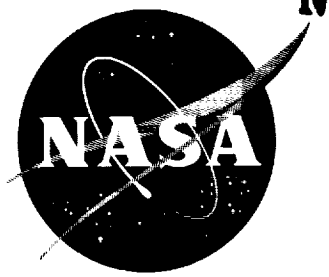

TECHNICAL NOTE

D-1741

THEORETICAL ELASTIC STRESS DISTRIBUTIONS IN CASSINIAN DOMES

By David A. Spera and Robert H. Johns

Lewis Research Center
Cleveland, Ohio

NATIONAL AERONAUTICS AND SPACE ADMINISTRATION
WASHINGTON
July 1963

NATIONAL AERONAUTICS AND SPACE ADMINISTRATION

TECHNICAL NOTE D-1741

THEORETICAL ELASTIC STRESS DISTRIBUTIONS IN CASSINIAN DOMES

By David A. Spera and Robert H. Johns

SUMMARY

The geometric properties and elastic stress distributions in a family of domes with constant thickness, temperature, internal pressure, and material properties are investigated, and results are presented in a form suitable for preliminary design. The governing differential equations are solved by a finite-difference technique, which is presented in detailed algebraic form for the shells investigated and in matrix form for general shells of revolution.

Meridians of the domes considered are modified curves of Cassini and contain two parameters that permit a wide range of shapes. Variations in dome curvature, height, area, and volume with these two parameters are calculated. Membrane stress distributions and significant bending stresses are given for a class of domes that close cylinders of equal thickness and have zero curvature at the junction section. Complete stress distributions are found for several dome geometries. In addition, a dome was fabricated and tested, and good agreement between experimental and theoretical results was obtained. By utilizing the shape flexibility of Cassinian domes, discontinuity stresses may be minimized through judicious selection of shape parameters and wall thickness.

INTRODUCTION

As part of a general program to determine stresses in thin-walled shells of revolution used in aircraft, missile, and space vehicle structures, a variety of cylinder closures has been investigated (ref. 1). In general, discontinuity stresses in these shells were significant. The present work is an investigation of a family of domes that show promise of reducing discontinuity effects.

Flügge (refs. 2 and 3) has proposed a series of domes generated by modified curves of Cassini. These modified curves contain two parameters that permit a wide variation in curvature throughout their lengths. Ellipses are included as special cases. Because domes generated by these curves, hereinafter called Cassinian domes, have a wide range of edge deformations under load, including those of equal thickness membrane cylinders, they were selected for this investigation.

References 2 and 3 present a membrane analysis of the Cassinian dome, which was expanded upon in reference 4 to include a more detailed description of the

two-parameter characteristics of the shells. In these references, free-edge deflection is assumed to depend upon the meridional curvature only at the dome boundary, and free-edge rotation is assumed to be zero. Although both these assumptions were consistent with the membrane analysis used, they were approximations that did not necessarily predict edge deformations with sufficient accuracy, as noted in references 5 and 6. Bending moments also exist at the apex of the dome, which may be the critical region for design. With the limitations of the membrane analysis in mind, further study including bending effects seemed necessary for a complete understanding of Cassinian domes.

In this investigation, stresses are computed using the equations proposed in reference 7 for a general thin-walled shell of revolution. A finite-difference solution of these equations is given in reference 8 in matrix notation and is presented here in algebraic form for shells with constant thickness, temperature, internal pressure, and material properties. Reference 9 presents additional details of this method of analysis; preliminary results of the work herein are presented in reference 10.

The scope of this investigation includes calculation of detailed geometric properties of Cassinian domes, membrane and significant principal and effective stresses in a family of domes attached to cylinders of equal wall thickness, and complete stress distributions for a selected dome. The family of domes has zero curvature at its junction section. Thus, any abrupt change in curvature between dome and cylinder is eliminated, and discontinuity stresses are greatly reduced. In addition to this theoretical work, a small-scale Cassinian dome with an integrally machined section of cylinder was tested, and the results are included in reference 10 and in this report.

SYMBOLS

A,B,F,J,P,R	matrices, 2×2
a	radius of cylinder, in.
C	extensional rigidity, Eh, lb/in.
D	flexural rigidity, $Eh^3/12(1 - \nu^2)$, lb-in.
E	modulus of elasticity, psi
g,k,q,t,y	matrices, 2×1
H	radial stress resultant, lb/in.
h	thickness of shell wall, in.
$\bar{j}$	dome station nearest to junction
$\breve{j}$	boundary station
M	couple, lb-in./in.

m,n	Cassinian dome shape parameters
N	tangential stress resultant, lb/in.
p	internal pressure, lb/sq in.
Q	transverse stress resultant, lb/in.
r	radial coordinate to middle surface, in.
S	surface area of dome, sq in.
s	meridional coordinate along middle surface, in.
u	radial deflection, in.
V	axial stress resultant, lb/in.
v	volume of dome, cu in.
x,z	axial coordinates to middle surface, in. (fig. 1)
α_o	reference length, in.
β	meridional rotation, radians
$\Gamma,\Theta,\Lambda,\Upsilon,\Phi,\Psi$	coefficients
δ	arc length from station $\overline{j}$ to junction, in.
ϵ	normal strain, in./in.
μ,η	constants
λ_1,λ_2	load terms, $(\text{in.-lb})^{1/2}$
ν	Poisson's ratio
ξ	s/α_o
ρ	curvature, $(\text{in.})^{-1}$
σ	normal stress, psi
φ	meridional slope, radians

Subscripts:

e	effective

H radial

is inner surface

j station along shell meridian

max maximum

min minimum

o apex, r = 0

os outer surface

V axial

θ circumferential

ξ meridional

Superscripts:

$\bar{\ }$ junction

$( )'$ differentiation with respect to ξ

GEOMETRY

The basic equation of the Cassinian dome meridian (ref. 4 and fig. 1) is

$$(r^2 + n^2x^2)^2 + 2ma^2(r^2 - n^2x^2) = a^4(1 + 2m) \tag{1}$$

Solving equation (1) for x and for r, explicitly, gives

$$x = \frac{a}{n}\sqrt{m - \left(\frac{r}{a}\right)^2 + \sqrt{(1 + m)^2 - 4m\left(\frac{r}{a}\right)^2}} \tag{2a}$$

and

$$r = a\sqrt{-m - n^2\left(\frac{x}{a}\right)^2 + \sqrt{(1 + m)^2 + 4mn^2\left(\frac{x}{a}\right)^2}} \tag{2b}$$

Dome height and meridional curvatures at junction and apex are, respectively,

$$x_o = \frac{a}{n}\sqrt{1 + 2m} \tag{3a}$$

$$\overline{\rho}_{\xi} = \left\{ \frac{-\frac{d^2r}{dx^2}}{\left[1 + \left(\frac{dr}{dx}\right)^2\right]^{3/2}} \right\}_{a,0} = -\left(\frac{d^2r}{dx^2}\right)_{a,0} = \frac{n^2}{a}\frac{1 - m}{1 + m} \tag{3b}$$

and

$$\rho_o = \left\{ \frac{-\frac{d^2x}{dr^2}}{\left[1 + \left(\frac{dx}{dr}\right)^2\right]^{3/2}} \right\}_{0,x_o} = -\left(\frac{d^2x}{dr^2}\right)_{0,x_o} = \frac{1}{an\sqrt{1 + 2m}}\frac{1 + 3m}{1 + m} \tag{3c}$$

It can be seen from equations (3b) and (3c) that m is limited to the range $-1/3$ to 1 for domes of positive Gaussian curvature. If $m = 0$, equation (1) describes a family of ellipses. Figure 2(a) shows several Cassinian dome meridians with various combinations of shape parameters m and n. Figures 2(b) to (e) contain additional details of the geometry of Cassinian domes and, with figure 2(a), are treated further in RESULTS AND DISCUSSION.

ANALYTICAL PROCEDURE

All stress resultants and moments in the dome may be found from the quantities H and β (fig. 1). Differential equations appropriate to thin elastic shells have been presented by Reissner (ref. 7) and are given here in modified notation without proof:

$$\left.\begin{aligned} (rH)'' + \Gamma(rH)' + \Theta(rH) + \Lambda\beta &= \lambda_1 \\ \text{and} \qquad \beta'' + \Upsilon\beta' + \Phi\beta + \Psi(rH) &= \lambda_2 \end{aligned}\right\} \tag{4}$$

The primes denote differentiation with respect to the nondimensional meridional coordinate ξ.

For a thin elastic shell with constant wall thickness, internal pressure, and material properties, the coefficients in equations (4) are

$$
\left.
\begin{aligned}
\Gamma &= \frac{a}{r}\cos\varphi \\
\Theta &= -a^2\left[\left(\frac{\cos\varphi}{r}\right)^2 - \nu\rho_\xi\rho_\theta\right] \\
\Lambda &= -a^2\rho_\theta Eh \\
\Upsilon &= \Gamma \\
\Phi &= -a^2\left[\left(\frac{\cos\varphi}{r}\right)^2 + \nu\rho_\xi\rho_\theta\right] \\
\Psi &= \frac{12(1-\nu^2)}{Eh^3}a^2\rho_\theta \\
\lambda_1 &= -\frac{pa^2}{2}r\cos\varphi\left[3\rho_\theta + (2-\nu)\rho_\xi\right] \\
\lambda_2 &= 6(1-\nu^2)\frac{pa^2}{Eh^3}r\cos\varphi
\end{aligned}
\right\} \qquad (5)
$$

Appendixes A, B, and C present expressions for these coefficients for a general shell of revolution, a numerical solution of equations (4), and methods for calculating stresses and strains from (rH) and β. An electronic computer was used to carry out this numerical solution.

RESULTS AND DISCUSSION

Geometry and Membrane Stresses

Selection of a dome of maximum efficiency for a given application may be made to some extent on the basis of a membrane analysis. However, since the membrane solution for pseudoelliptical shells may be significantly in error (ref. 5), this selection should be considered as preliminary only. A more complete analysis based on the analytical methods described in this report and in reference 8 may be used to modify this initial selection of dome parameters. Figures 2(b) to (f) are presented, therefore, as a description of the membrane Cassinian dome that is useful in preliminary design.

In general, three regions of the dome surface are of special interest: the apex region, the knuckle region, and the junction region. The knuckle region is not always as clearly defined as that of the apex or junction. In this report, the knuckle region is defined as that interior section of the dome in which the circumferential stress may reach a minimum value. This region is of particular

interest when this minimum stress is compressive, and buckling or high effective stress may result.

Figure 2(b) presents data on the apex and junction regions. The nondimensional radius of curvature at the apex may be determined from the desired membrane effective stress in that region by the formula

$$\frac{1}{a\rho_o} = \frac{\sigma_{e,o}}{\frac{pa}{2h}} \tag{6}$$

If $1/a\rho_o$ equals 1.732, membrane effective stress at the dome apex is equal to that of a cylinder of equal thickness. The meridional curvature at the junction, $\overline{\rho}_\xi$, is one of the factors influencing edge deflection and rotation of the shell and can be determined approximately from the desired junction deflection by the membrane formula

$$a\overline{\rho}_\xi = (2 - \nu) - \frac{\overline{u}}{\frac{pa^2}{2Eh}} \tag{7}$$

Lines of constant minimum membrane circumferential stress $\sigma_{\theta,min}$ are included in figure 2(c) to aid in determining whether or not buckling may occur in the dome. The left and right segments of the curves indicate minimum membrane stresses occurring in the knuckle region. These sections of the curves are obtained by cross-plotting results from analyses of many domes because no formula for them is available. The central segments show stresses that are minimum at the junction. These membrane stresses may be calculated from the meridional curvature at the junction by the formula

$$\frac{\overline{\sigma}_\theta}{\frac{pa}{h}} = 1 - \frac{a\overline{\rho}_\xi}{2} \tag{8}$$

Substituting equation (3b) into (8) gives the relation between the membrane circumferential stress at the junction and the parameters m and n. Often, $\sigma_{\theta,min}$ and $\sigma_{e,o}$ are the most important considerations in the preliminary selection of a shallow dome. Figure 2(c) also shows the variation in dome height with m and n.

Other observations concerning Cassinian dome geometry and membrane stresses may be made from equation (1) and figures 2(a), (b), and (c):

(1) If $m = -0.333$, the dome is flat at the apex for all values of n, and apex stresses are theoretically infinite.

(2) In figure 2(a), the case with $m = -0.190$ and $n = 1.167$ is shown. This is the shallowest Cassinian dome with no membrane compression and with apex effective stress less than or equal to that in a membrane cylinder of equal thickness.

(3) If $m = 0$, the dome is ellipsoidal, and n equals the ratio of the radial semiaxis to the axial semiaxis. For this case, if $n = 1.0$, the dome is hemispherical. The ellipsoidal dome is the shallowest Cassinian dome for a given value of apex curvature and the deepest Cassinian dome for a given value of junction curvature.

In figure 2(a), the case with $m = 0$ and $n = 1.414$ is shown. This is the shallowest ellipsoidal shape without membrane compression.

(4) If $m = 1.0$, meridional curvature at the junction is zero for all values of n. These domes terminate in a section of a cylinder and have the largest nondimensional membrane junction deflection $\bar{u}/(pa^2/2Eh)$. In figure 2(a), the case with $m = 1.0$ and $n = 1.9$ is illustrated. This is the shallowest of the Cassinian domes with zero junction curvature and no membrane compression. The meridians with $m = 1.0$ and $n = 1.0$ and 3.0 are included to indicate the wide variety of shapes possible.

(5) If $n = 0$, the Cassinian equations describe a cylinder for all values of m.

When $a\bar{\rho}_\xi$ and $1/a\rho_o$ have been calculated using equations (6) and (7), m may be determined without the nonlinear interpolation required in figure 2(b). Using equations (3b) and (3c) gives

$$\frac{1 - m}{1 + 2m} \frac{(1 + 3m)^2}{(1 + m)^3} = (a\rho_o)^2(a\bar{\rho}_\xi) \tag{9}$$

Figure 2(d) shows the variation in m with $(a\rho_o)^2(a\bar{\rho}_\xi)$. Ambiguity is eliminated by determining the sign of m from figure 2(b); n may then be calculated from equation (3b) or (3c).

Figure 2(e) presents the variation in dome surface area and volume with m and n. The derivation of the equations for these quantities is given in appendix A.

Maximum membrane effective stresses, normalized with respect to the effective stress in a membrane cylinder, are given in figure 2(f). The regions in which these stresses occur are noted. It can be seen that, for most Cassinian domes of interest, knuckle region stresses are important because of their influence on buckling rather than for their contribution to the maximum membrane effective stress. In many applications, the dome stresses shown in this figure plus the membrane stresses in the structure adjoining the dome will be modified significantly by discontinuities.

In summary, the following procedure may be used to determine preliminary dome shape:

(1) For the given material, assume a dome wall thickness h.

(2) Calculate $1/a\rho_o$ and $a\bar{\rho}_\xi$ from the desired apex effective membrane

stress and junction deflection, respectively, using equations (6) and (7).

(3) Select initial values for m and n, using figures 2(b) and (d).

(4) Using figure 2(c), check to see if this initial geometry satisfies possible requirements on $\sigma_{\theta,min}$ and x_o, and modify $1/a\rho_o$ if necessary.

(5) Compute volume and weight of the total structure, using figure 2(e) for dome calculations.

(6) Repeat steps (1) to (5) to determine other combinations of h, m, n, and total structural weight. Select h for minimum weight.

(7) For complete stresses, perform detailed analysis using the described numerical solution to the basic shell equations. Modify the wall thickness h as necessary to remain within required maximum effective stress levels. Small changes in h should not affect overall structural weight significantly.

Stresses in a Family of Cylinder Closures

Figures 3 to 7 present theoretical results for the family of domes with parameter $m = 1$. Since these domes are characterized by zero meridional curvature at the junction section, they are particularly suited for use as end closures on cylinders of the same wall thickness.

The membrane stress distributions for these domes are given in figure 3, normalized with respect to the circumferential stress in a membrane cylinder. The smoothness of the curves across the junction section indicates the minimal character of any discontinuity effects that may be present. The presence of compressive stresses in domes with the larger values of parameter n causes an increase in effective stress in the knuckle regions.

Figures 4(a) to (c) show the variation in maximum effective stresses in the apex, knuckle, and junction regions with n and a/h for $m = 1$. In addition, critical effective stresses are included in figure 4(d). Again, these stresses are normalized with respect to the effective stress in a membrane cylinder. The results for a/h from 10 to about 30 should be considered as approximations in light of the thin-shell assumptions of this analysis. Figure 4(c) shows that, even though the meridional curvatures in dome and cylinder are equal at the junction, discontinuity effects are present, which indicates that meridional curvature only at the junction does not determine free-edge deformations completely.

The variation in minimum circumferential stress with n and a/h is given in figure 5. This information may be helpful in the design of ring stiffeners to prevent wrinkling or buckling of the dome wall.

Figures 6 and 7 give principal and effective stress distributions for domes with $m = 1.0$, $n = 1.9$, and various values of a/h. These are the shallowest Cassinian domes with zero junction curvature and no membrane compression. As in figure 4(c), discontinuity stresses in the junction region are noticeable, although they decrease rapidly as a/h increases.

Experimental Results

A small cylinder with a Cassinian dome was contour-machined from a 6061-T6 aluminum billet. The nominal outer diameter of the cylinder was 12.00 inches, and the nominal wall thickness was 0.062 inch. The dome shape parameters were $m = 1.0$ and $n = 1.9$ (fig. 2(a)). Experimental results and curves of theoretical stresses are presented in figure 8 for this test specimen. Reasonable agreement is obtained.

The test dome was selected because it combined zero junction curvature and zero minimum membrane stress, which eliminates curvature discontinuity and buckling. The shallowest ellipsoidal dome with no membrane compression has shape parameters $m = 0$ and $n = 1.414$. This ellipsoidal dome is compared geometrically with the test dome in figure 2(a). It can be seen that the two meridional curves are similar in shape, although the depth of the test dome is larger than that of the ellipsoidal dome. However, the test dome is nearly cylindrical for a portion of its depth, and interstage structures between propellant tanks with this type of dome would probably not extend from cylinder to cylinder. Also, the volume of the test dome is about 28 percent greater than that of the ellipsoidal dome. Effective stresses for the two domes are compared in figure 9, normalized with respect to the membrane effective stress in the adjoining cylinders. The maximum effective stress ratio arising from the ellipsoidal dome is 1.076 against 1.017 for the cylinder with the zero junction curvature dome. Thus, the theoretical yield pressure for the cylinder with the test dome is about 6 percent higher than that obtained using the comparable ellipsoidal dome. There is also considerably less bending in the knuckle region of the test dome, although apex stresses are higher but not critical. Figures 8 and 9 are discussed in reference 10 also.

CONCLUSIONS

Geometric properties and elastic stress distributions for Cassinian domes have been presented, and the following conclusions are drawn:

1. The Cassinian dome can be used to provide a family of cylinder closures with a wide range of shapes and a minimum amount of discontinuity stress. Included in this range are hemispherical and ellipsoidal domes.

2. Because the equation of the meridional curve of a Cassinian dome contains two parameters, much flexibility in meeting design conditions is possible.

3. Although matching the membrane edge deflections of the dome and adjoining structure reduces discontinuity effects considerably, bending moments and shears may still be present because of the approximate character of the membrane analysis.

4. Maximum effective stresses occur at the dome apex or in the region of the junction of the dome and adjoining structure in the majority of dome shapes of interest. Interior stresses are usually important only if they are compressive and may lead to buckling.

5. Testing of a fabricated Cassinian dome shows good agreement between experimental and theoretical stresses.

Lewis Research Center
National Aeronautics and Space Administration
Cleveland, Ohio, March 13, 1963

APPENDIX A

CALCULATION OF SHELL DATA

Station Coordinates and Curvatures

Since the basic differential equations (4) governing thin-shell deformations are to be solved using an equal-interval finite-difference method, it is first necessary to determine the coordinates of stations that divide the reference surface meridian into equal increments of arc. Referring to figure 1 and equations (1), (2a), and (2b) for $z \leq x_o$ gives

$$\left.\begin{aligned} z_j = x_o - x_j &= x_o - \frac{1}{n}\sqrt{ma^2 - r_j^2 + a\sqrt{a^2(1+m)^2 - 4mr_j^2}} \\ \left(\frac{dz}{dr}\right)_j &= -\left(\frac{dx}{dr}\right)_j = \frac{r_j}{n^2(x_o - z_j)}\left[1 + \frac{2ma}{\sqrt{a^2(1+m)^2 - 4mr_j^2}}\right] \\ \varphi_j &= \tan^{-1}\left(\frac{dz}{dr}\right)_j \\ r_{j+1} &= r_{j-1} + 2\alpha_o(\Delta\xi)\cos\varphi_j \end{aligned}\right\} \quad \text{(A1)}$$

Also,

$$\left.\begin{aligned} r_j &= \sqrt{-\left[n^2(x_o - z_j)^2 + ma^2\right] + a\sqrt{a^2(1+m)^2 + 4mn^2(x_o - z_j)^2}} \\ \left(\frac{dr}{dz}\right)_j &= -\left(\frac{dr}{dx}\right)_j = \frac{n^2(x_o - z_j)}{r_j}\left[1 - \frac{2ma}{\sqrt{a^2(1+m)^2 + 4mn^2(x_o - z_j)^2}}\right] \\ \varphi_j &= \cot^{-1}\left(\frac{dr}{dz}\right)_j \\ z_{j+1} &= z_{j-1} + 2\alpha_o(\Delta\xi)\sin\varphi_j \end{aligned}\right\} \quad \text{(A2)}$$

To begin the calculation of coordinates, r_1, φ_1, and r_2 are determined from the boundary conditions on the meridian curve. Equations (A1) and (A2) are then used to calculate the remaining coordinates. To avoid difficulties with large values of dz/dr and dr/dz, equations (A2) are used when φ is larger than $\pi/4$. In practice, it is desirable to divide the shell meridian into increments of length $\alpha_o(\Delta\xi)/2$ and then to use the odd-numbered stations. This pro-

cedure will avoid incremental lengths that are alternately slightly larger and slightly smaller than $\alpha_o(\Delta\xi)$.

To calculate the curvatures of the reference surface, the following equations are used when $z \leq x_o$:

$$\left.\begin{aligned} \rho_{\xi,1} = \rho_{\theta,1} = \rho_o &= \frac{1}{an\sqrt{1+2m}}\left(\frac{1+3m}{1+m}\right) \\ \rho_{\xi,j} = \left(\frac{d\varphi}{ds}\right)_j &= \frac{(\varphi_{j+1} - \varphi_{j-1})}{2\alpha_o(\Delta\xi)} \qquad j = 2,\bar{j}-1 \\ \rho_{\xi,\bar{j}} &= \frac{\frac{\pi}{2} - \varphi_{\bar{j}-1}}{2\alpha_o(\Delta\xi)} \\ \rho_{\theta,j} &= \frac{\sin\varphi_j}{r_j} \qquad j = 2,\bar{j} \end{aligned}\right\} \tag{A3}$$

When $z > x_o$,

$$\left.\begin{aligned} z_j &= z_{j-1} + \alpha_o(\Delta\xi) \\ r_j &= a \\ \varphi_j &= \frac{\pi}{2} \\ \rho_{\xi,j} &= 0 \\ \rho_{\theta,j} &= \frac{1}{a} \qquad j = \bar{j}+1,\breve{j} \end{aligned}\right\} \tag{A4}$$

Coefficients in the Basic Differential Equations

For a general shell of revolution, the coefficients in equations (4) are given in reference 7 as

$$
\left.
\begin{aligned}
\Gamma &= \frac{(r/C\alpha_o)'}{r/C\alpha_o} \\
\Theta &= -\left[\left(\frac{r'}{r}\right)^2 + \nu\,\frac{(r'/C\alpha_o)'}{r/C\alpha_o}\right] \\
\Lambda &= -\,\frac{z'}{r/C\alpha_o} \\
\Upsilon &= \frac{(rD/\alpha_o)'}{rD/\alpha_o} \\
\Phi &= -\left[\left(\frac{r'}{r}\right)^2 - \nu\,\frac{(r'D/\alpha_o)'}{rD/\alpha_o}\right] \\
\Psi &= \frac{z'}{rD/\alpha_o} \\
\lambda_1 &= -\left\{\left[\frac{(r/C\alpha_o)'}{r/C\alpha_o} + \nu\,\frac{r'}{r}\right](r\alpha_o p_H) + (r\alpha_o p_H)'\right\} \\
&\quad + \left\{\left[\frac{z'r'}{r^2} + \nu\,\frac{(z'/C\alpha_o)'}{r/C\alpha_o}\right](rV) + \nu\left(\frac{z'}{r}\right)(rV)'\right\} \\
\lambda_2 &= \frac{r'(rV)}{rD/\alpha_o}
\end{aligned}
\right\} \quad \text{(A5)}
$$

In these equations,

$$r' = \alpha_o \cos\varphi$$

$$r'' = -\alpha_o^2 \rho_\xi \sin\varphi$$

$$z' = \alpha_o \sin\varphi$$

$$z'' = \alpha_o^2 \rho_\xi \cos\varphi$$

and

$$(rV) = -\int_{\xi} r\alpha_o p_V \, d\xi$$

For constant internal pressure,

$$(rV) = \frac{pr^2}{2}$$

and

$$p_H = p \sin \varphi$$

Therefore, for constant wall thickness, internal pressure, and material properties, and with $\alpha_o = a$, equations (A5) reduce to equations (5).

Dome Surface Area

The dome surface area (fig. 1(a)) is

$$S \approx \pi\left(\frac{r_2}{2}\right)^2 + \sum_{j=2}^{\bar{j}-1} 2\pi r_j(\Delta s) + 2\pi r_{\bar{j}}\left(\frac{\Delta s}{2} + \delta\right)$$

Now

$$r_2 \approx \Delta s = a(\Delta\xi)$$

and

$$r_{\bar{j}} \approx a$$

Therefore,

$$\frac{S}{a^2} \approx 2\pi(\Delta\xi)\left[\sum_{j=2}^{\bar{j}-1}\left(\frac{r_j}{a}\right) + \frac{5}{8}(\Delta\xi) + \frac{\delta}{a(\Delta\xi)}\right] \tag{A6}$$

This equation is used to compute the dome surface areas shown in figure 2(e).

Dome Volume

The volume enclosed by the reference surface of a Cassinian dome (fig. 1(a))

is

$$v = 2\pi \int_0^a xr\ dr = \pi \int_0^{a^2} x\ d(r^2)$$

or

$$\frac{v}{a^3} = \pi \int_0^1 \left(\frac{x}{a}\right) d\left(\frac{r}{a}\right)^2$$

$$\left(\frac{r}{a}\right)^2 = -n^2\left(\frac{x}{a}\right)^2 - m + \sqrt{(1+m)^2 + 4mn^2\left(\frac{x}{a}\right)^2}$$

Therefore,

$$\frac{v}{a^3} = -\pi n^2 \int_{(x_o/a)^2}^0 \sqrt{\left(\frac{x}{a}\right)^2}\ d\left(\frac{x}{a}\right)^2 + 2\pi mn^2 \int_{(x_o/a)^2}^0 \frac{\sqrt{\left(\frac{x}{a}\right)^2}\ d\left(\frac{x}{a}\right)^2}{\sqrt{(1+m)^2 + 4mn^2\left(\frac{x}{a}\right)^2}}$$

Let

$$(1+m)^2 = \alpha$$

$$4mn^2 = \beta$$

$$\left(\frac{x}{a}\right)^2 = \gamma$$

and

$$\left(\frac{x_o}{a}\right)^2 = \gamma_o$$

Then

$$\frac{v}{a^3} = -\pi n^2 \int_{\gamma_o}^0 \sqrt{\gamma}\ d\gamma + \frac{\pi\beta}{2} \int_{\gamma_o}^0 \frac{\sqrt{\gamma}\ d\gamma}{\sqrt{\alpha + \beta\gamma}} \qquad \text{(A7)}$$

From reference 11 and equation (3a), for $\beta > 0$, equation (A7) becomes

$$\frac{v}{a^3} = \pi\left\{\frac{2n^2\gamma_o^{3/2}}{3} + \frac{1}{2}\left[-\sqrt{\alpha\gamma_o + \beta\gamma_o^2} + \frac{\alpha}{\sqrt{\beta}}\ln\left(\frac{\sqrt{\alpha\beta + \beta^2\gamma_o} + \beta\sqrt{\gamma_o}}{\sqrt{\alpha\beta}}\right)\right]\right\}$$

or

$$\frac{v}{a^3} = \frac{\pi}{n}\left\{\frac{(1 - m)\sqrt{1 + 2m}}{6} + \frac{(1 + m)^2}{4\sqrt{m}}\ln\left[\frac{1 + 3m + 2\sqrt{m(1 + 2m)}}{1 + m}\right]\right\} \qquad \text{for } m > 0 \tag{A8}$$

Taking the limit of v/a^3 as β approaches zero,

$$\frac{v}{a^3} = \frac{2\pi}{3n} \qquad \text{for } m = 0 \tag{A9}$$

For $\beta < 0$, equation (A7) becomes

$$\frac{v}{a^3} = \pi\left\{\frac{2n^2\gamma_o^{3/2}}{3} + \frac{1}{2}\left[-\sqrt{\alpha\gamma_o + \beta\gamma_o^2} + \frac{\alpha}{2\sqrt{-\beta}}\left(\frac{\pi}{2} - \sin^{-1}\frac{2\beta\gamma_o + \alpha}{\alpha}\right)\right]\right\}$$

or

$$\frac{v}{a^3} = \frac{\pi}{n}\left\{\frac{(1 - m)\sqrt{1 + 2m}}{6} + \frac{(1 + m)^2}{8\sqrt{-m}}\cos^{-1}\left[1 + \frac{8m(1 + 2m)}{(1 + m)^2}\right]\right\} \qquad \text{for } m < 0 \tag{A10}$$

Equations (A8), (A9), and (A10) are used to compute the dome volumes given in figure 2(e).

APPENDIX B

SOLUTION OF DIFFERENTIAL EQUATIONS

At any station j on the middle surface meridian curve, equations (4) become

$$\left.\begin{aligned} (rH)''_j + \Gamma_j (rH)'_j + \Theta_j (rH)_j + \Lambda_j \beta_j &= \lambda_{1,j} \\ \beta''_j + \Upsilon_j \beta'_j + \Phi_j \beta_j + \Psi_j (rH)_j &= \lambda_{2,j} \end{aligned}\right\} \tag{B1}$$

In finite-difference form, using central differences and incremental length $(\Delta\xi)$,

$$(rH)''_j = \frac{(rH)_{j+1} - 2(rH)_j + (rH)_{j-1}}{(\Delta\xi)^2}, \quad . \quad . \quad . \tag{B2}$$

Substituting equations (B2) into (B1), with $j = 1$ and $j = \breve{j}$ at the boundaries, gives

$$\left.\begin{aligned} (rH)_{j+1}\left[1 + \frac{(\Delta\xi)}{2}\Gamma_j\right] + (rH)_j\left[-2 + (\Delta\xi)^2\Theta_j\right] + (rH)_{j-1}\left[1 - \frac{(\Delta\xi)}{2}\Gamma_j\right] \\ + (\Delta\xi)^2\Lambda_j\beta_j = (\Delta\xi)^2\lambda_{1,j} \\ \beta_{j+1}\left[1 + \frac{(\Delta\xi)}{2}\Upsilon_j\right] + \beta_j\left[-2 + (\Delta\xi)^2\Phi_j\right] + \beta_{j-1}\left[1 - \frac{(\Delta\xi)}{2}\Upsilon_j\right] \\ + (\Delta\xi)^2\Psi_j(rH)_j = (\Delta\xi)^2\lambda_{2,j} \qquad j = 2, \breve{j} - 1 \end{aligned}\right\} \tag{B3}$$

In matrix notation, with capital letters for 2×2 matrices and lower-case letters for 2×1 matrices, equations (B3) become

$$A_j y_{j+1} + B_j y_j + F_j y_{j-1} = g_j, \qquad j = 2, \breve{j} - 1 \tag{B4}$$

in which

$$
\left.
\begin{aligned}
y_j &= \begin{bmatrix} (rH)_j \\ \beta_j \end{bmatrix} \\
A_j &= \begin{bmatrix} 1 + \frac{(\Delta\xi)}{2}\Gamma_j & 0 \\ 0 & 1 + \frac{(\Delta\xi)}{2}\Upsilon_j \end{bmatrix} = \begin{bmatrix} a_{11,j} & 0 \\ 0 & a_{22,j} \end{bmatrix} \\
B_j &= \begin{bmatrix} -2 + (\Delta\xi)^2\Theta_j & (\Delta\xi)^2\Lambda_j \\ (\Delta\xi)^2\Psi_j & -2 + (\Delta\xi)^2\Phi_j \end{bmatrix} = \begin{bmatrix} b_{11,j} & b_{12,j} \\ b_{21,j} & b_{22,j} \end{bmatrix} \\
F_j &= \begin{bmatrix} 1 - \frac{(\Delta\xi)}{2}\Gamma_j & 0 \\ 0 & 1 - \frac{(\Delta\xi)}{2}\Upsilon_j \end{bmatrix} = \begin{bmatrix} f_{11,j} & 0 \\ 0 & f_{22,j} \end{bmatrix} \\
g_j &= \begin{bmatrix} (\Delta\xi)^2\lambda_{1,j} \\ (\Delta\xi)^2\lambda_{2,j} \end{bmatrix} = \begin{bmatrix} g_{1,j} \\ g_{2,j} \end{bmatrix}
\end{aligned}
\right\} \qquad \text{(B5)}
$$

Following the method of reference 8, let

$$y_j = q_j - P_j y_{j+1} \qquad \text{(B6a)}$$

then

$$y_{j-1} = q_{j-1} - P_{j-1} y_j \qquad \text{(B6b)}$$

and

$$y_{j+1} = P_j^{-1}(q_j - y_j) \qquad \text{(B6c)}$$

Substituting equations (B6b) and (B6c) into (B4) gives

$$A_j P_j^{-1}(q_j - y_j) + B_j y_j + F_j(q_{j-1} - P_{j-1} y_j) = g_j$$

or

$$(-A_jP_j^{-1} + B_j - F_jP_{j-1})y_j + (A_jP_j^{-1}q_j + F_jq_{j-1}) = g_j, \qquad j = 2,\breve{j} - 1$$

As is shown later, P_j and q_j are independent of the boundary conditions at $j = \breve{j}$, but y_j is not. Therefore,

$$\left.\begin{aligned} -A_jP_j^{-1} + B_j - F_jP_{j-1} &= 0 \\ \text{and} \\ A_jP_j^{-1}q_j + F_jq_{j-1} &= g_j, \qquad j = 2,\breve{j} - 1 \end{aligned}\right\} \tag{B7}$$

Solving equations (B7) for P_j and q_j results in

$$\left.\begin{aligned} P_j &= (B_j - F_jP_{j-1})^{-1} A_j \\ \text{and} \\ q_j &= P_jA_j^{-1}(g_j - F_jq_{j-1}), \qquad j = 2,\breve{j} - 1 \end{aligned}\right\} \tag{B8}$$

General boundary conditions may be expressed as

$$\left.\begin{aligned} (rH)_1 &= k_1 - j_{11}(rH)_2 - j_{12}\beta_2 \\ \beta_1 &= k_2 - j_{21}(rH)_2 - j_{22}\beta_2 \\ (rH)_{\breve{j}} &= t_1 - r_{11}(rH)_{\breve{j}-1} - r_{12}\beta_{\breve{j}-1} \\ \beta_{\breve{j}} &= t_2 - r_{21}(rH)_{\breve{j}-1} - r_{22}\beta_{\breve{j}-1} \end{aligned}\right\} \tag{B9}$$

Expressing equations (B9) in matrix form gives

$$y_1 = k - Jy_2 \tag{B10a}$$

$$y_{\breve{j}} = t - Ry_{\breve{j}-1} \tag{B10b}$$

Comparing (B6a) and (B10a) yields

$$\left.\begin{aligned} P_1 &= J \\ q_1 &= k \end{aligned}\right\} \tag{B11}$$

Using equations (B6b) and (B10b) results in

$$R(q_{\breve{j}-1} - P_{\breve{j}-1}y_{\breve{j}}) + y_{\breve{j}} = t$$

or

$$\underset{\sim}{y}_j = (I - R\underset{\sim}{P}_{j-1})^{-1}(t - R\underset{\sim}{q}_{j-1}) \tag{B12}$$

in which I equals the 2×2 identity matrix.

To expand equations (B6a), (B8), (B11), and (B12) into algebraic form, let

$$P_j = \begin{bmatrix} p_{11,j} & p_{12,j} \\ p_{21,j} & p_{22,j} \end{bmatrix}$$

and

$$q_j = \begin{bmatrix} q_{1,j} \\ q_{2,j} \end{bmatrix}$$

Then

$$\left.\begin{aligned}
p_{11,1} &= j_{11} \\
p_{12,1} &= j_{12} \\
p_{21,1} &= j_{21} \\
p_{22,1} &= j_{22} \\
P_{11,j} &= \eta_j a_{11,j}(b_{22,j} - f_{22,j}p_{22,j-1}) \\
P_{12,j} &= -\eta_j a_{22,j}(b_{12,j} - f_{11,j}p_{12,j-1}) \\
p_{21,j} &= -\eta_j a_{11,j}(b_{21,j} - f_{22,j}p_{21,j-1}) \\
p_{22,j} &= \eta_j a_{22,j}(b_{11,j} - f_{11,j}p_{11,j-1})
\end{aligned}\right\} \tag{B13}$$

in which

$$\eta_j = \left[(b_{11,j} - f_{11,j}p_{11,j-1})(b_{22,j} - f_{22,j}p_{22,j-1}) - (b_{12,j} - f_{11,j}p_{12,j-1})(b_{21,j} - f_{22,j}p_{21,j-1})\right]^{-1}$$

and

$$\left.\begin{aligned}
q_{1,1} &= k_1 \\
q_{2,1} &= k_2 \\
q_{1,j} &= \frac{p_{11,j}}{a_{11,j}}(g_{1,j} - f_{11,j}q_{1,j-1}) + \frac{p_{12,j}}{a_{22,j}}(g_{2,j} - f_{22,j}q_{2,j-1}) \\
q_{2,j} &= \frac{p_{21,j}}{a_{11,j}}(g_{1,j} - f_{11,j}q_{1,j-1}) + \frac{p_{22,j}}{a_{22,j}}(g_{2,j} - f_{22,j}q_{2,j-1}) \\
& \qquad\qquad j = 2, \check{j} - 1
\end{aligned}\right\}$$

Finally,

$$
\left.
\begin{aligned}
(rH)_{\check{j}} &= \mu\Big[(1 - r_{21}p_{12,\check{j}-1} - r_{22}p_{22,\check{j}-1})(t_1 - r_{11}q_{1,\check{j}-1} - r_{12}q_{2,\check{j}-1}) \\
&\qquad + (r_{11}p_{12,\check{j}-1} + r_{12}p_{22,\check{j}-1})(t_2 - r_{21}q_{1,\check{j}-1} - r_{22}q_{2,\check{j}-1})\Big] \\
\beta_{\check{j}} &= \mu\Big[(1 - r_{11}p_{11,\check{j}-1} - r_{12}p_{21,\check{j}-1})(t_2 - r_{21}q_{1,\check{j}-1} - r_{22}q_{2,\check{j}-1}) \\
&\qquad + (r_{21}p_{11,\check{j}-1} - r_{22}p_{21,\check{j}-1})(t_1 - r_{11}q_{1,\check{j}-1} - r_{12}q_{2,\check{j}-1})\Big]
\end{aligned}
\right\} \quad \text{(B14)}
$$

in which

$$
\mu = \Big[(1 - r_{11}p_{11,\check{j}-1} - r_{12}p_{21,\check{j}-1})(1 - r_{21}p_{12,\check{j}-1} - r_{22}p_{22,\check{j}-1}) - (r_{11}p_{12,\check{j}-1} + r_{12}p_{22,\check{j}-1})(r_{21}p_{11,\check{j}-1} + r_{22}p_{21,\check{j}-1})\Big]^{-1}
$$

and

$$
\left.
\begin{aligned}
(rH)_j &= q_{1,j} - p_{11,j}(rH)_{j+1} - p_{12,j}\beta_{j+1} \\
\beta_j &= q_{2,j} - p_{21,j}(rH)_{j+1} - p_{22,j}\beta_{j+1} \qquad j = \check{j} - 1,1
\end{aligned}
\right\}
$$

To solve the shell equations:

(1) Calculate the elements of the A, B, F, g, J, k, R, and t matrices, using equations (B5) and (B9).

(2) Calculate the elements of the P and q matrices, using equations (B13) and traversing the shell meridian from station 1 to station $\check{j} - 1$.

(3) Calculate (rH) and β, using equations (B14) and traversing the shell meridian from station $\check{j}$ to station 1.

It can be seen that the boundary conditions at station $\check{j}$ are not used until step (3). Therefore, P and q are indeed independent of these boundary conditions, as previously assumed.

APPENDIX C

CALCULATION OF STRESSES AND STRAINS

Referring to figure 1 and reference 7,

$$\left.\begin{aligned} N_\xi &= V \sin \varphi + H \cos \varphi = -\rho_\theta \int_\xi r\alpha_o p_V \, d\xi + (rH) \frac{\cos \varphi}{r} \\ N_\theta &= \frac{(rH)'}{\alpha_o} + r p_H \\ M_\xi &= \frac{D}{\alpha_o}\left(\beta' + \nu \frac{r'}{r} \beta\right) \\ M_\theta &= \frac{D}{\alpha_o}\left(\nu\beta' + \frac{r'}{r} \beta\right) \end{aligned}\right\} \qquad (C1)$$

In finite-difference form, for $\alpha_o = a$ and for constant internal pressure, wall thickness, and material properties, equations (C1) become

$$\left.\begin{aligned} N_{\xi,j} &= \frac{p}{2} r_j \sin \varphi_j + (rH)_j \frac{\cos \varphi_j}{r_j} \\ N_{\theta,j} &= p r_j \sin \varphi_j + \frac{1}{2\alpha_o(\Delta\xi)}\left[(rH)_{j+1} - (rH)_{j-1}\right] \\ M_{\xi,j} &= \frac{D}{\alpha_o}\left[\frac{(\beta_{j+1} - \beta_{j-1})}{2(\Delta\xi)} + \nu \frac{\alpha_o \cos \varphi_j}{r_j} \beta_j\right] \\ M_{\theta,j} &= \frac{D}{\alpha_o}\left[\nu \frac{(\beta_{j+1} - \beta_{j-1})}{2(\Delta\xi)} + \alpha_o \frac{\cos \varphi_j}{r_j} \beta_j\right] \qquad j = 2, \breve{j} - 1 \end{aligned}\right\} \qquad (C2)$$

To calculate the stress resultants and couples at $j = 1$ when $r_1 = 0$, the following procedure is used: Let W_1 represent the desired function and W_{-2} represent the function at the station a distance (Δs) from the apex along a meridian 180° from the nominal meridian. Since the functions (C2) are even for a closed shell,

$$W_{-2} = W_2$$

and

$$W_1' = 0$$

Selecting the appropriate numerical differentiation formula from reference 12 for the first derivative of a function that is known at four points results in

$$W_1' = \frac{-2W_{-2} - 3W_1 + 6W_2 - W_3}{6(\Delta\xi)} = 0$$

Therefore, for a closed dome,

$$W_1 = \frac{4}{3} W_2 - \frac{1}{3} W_3 \tag{C3}$$

Other boundary conditions may be handled in a similar manner.

To calculate stresses and strains, the following formulas are used:

$$\left.\begin{aligned}
\sigma_{\xi,\begin{Bmatrix}is\\os\end{Bmatrix}} &= \frac{N_\xi}{h} \pm 6\,\frac{M_\xi}{h^2} \\
\sigma_{\theta,\begin{Bmatrix}is\\os\end{Bmatrix}} &= \frac{N_\theta}{h} \pm 6\,\frac{M_\theta}{h^2} \\
\sigma_{e,\begin{Bmatrix}is\\os\end{Bmatrix}} &= \sqrt{\sigma^2_{\xi,\begin{Bmatrix}is\\os\end{Bmatrix}} - \sigma_{\xi,\begin{Bmatrix}is\\os\end{Bmatrix}}\sigma_{\theta,\begin{Bmatrix}is\\os\end{Bmatrix}} + \sigma^2_{\theta,\begin{Bmatrix}is\\os\end{Bmatrix}}} \\
\epsilon_{\xi,\begin{Bmatrix}is\\os\end{Bmatrix}} &= \frac{1}{E}\left(\sigma_{\xi,\begin{Bmatrix}is\\os\end{Bmatrix}} - \nu\sigma_{\theta,\begin{Bmatrix}is\\os\end{Bmatrix}}\right) \\
\epsilon_{\theta,\begin{Bmatrix}is\\os\end{Bmatrix}} &= \frac{1}{E}\left(\sigma_{\theta,\begin{Bmatrix}is\\os\end{Bmatrix}} - \nu\sigma_{\xi,\begin{Bmatrix}is\\os\end{Bmatrix}}\right)
\end{aligned}\right\} \tag{C4}$$

REFERENCES

1. Johns, Robert H., and Orange, Thomas W.: Theoretical Elastic Stress Distributions Arising from Discontinuities and Edge Loads in Several Shell-Type Structures. NASA TR R-103, 1961.

2. Flügge, W.: Stress Problems in Pressurized Cabins. NACA TN 2612, 1952.

3. Flügge, W.: Stresses in Shells. Springer-Verlag (Berlin), 1960.

4. Read, W. S.: Cassinian Domes for Pressure Vessel Design. Paper 62-Av-5, ASME, 1962.

5. Galletly, G. D.: Edge Influence Coefficients for Toroidal Shells of Positive Gaussian Curvature. Paper 59-Pet-2, ASME, 1959.

6. Galletly, G. D.: Bending of 2:1 and 3:1 Open-Crown Ellipsoidal Shells. Bull. Ser. 54, Welding Res. Council, 1959.

7. Reissner, Eric: On the Theory of Thin Elastic Shells. Reissner Anniversary Vol., Edwards Bros., Inc., 1959.

8. Radkowski, P. P., Davis, R. M., and Bolduc, M. R.: Numerical Analysis of Equations of Thin Shells of Revolution. ARS Jour., vol. 32, no. 1, Jan. 1962, pp. 36-41.

9. Wilson, P. E., and Spier, E. E.: Numerical Analysis of Small Finite Axisymmetric Deformation of Thin Shells of Revolution. ERR-AN-153, General Dynamics/Astronautics, 1962.

10. Johns, Robert H., Morgan, William C., and Spera, David A.: Theoretical and Experimental Analysis of Several Typical Junctions in Space Vehicle Structures. Paper 2427-62, Am. Rocket Soc., Inc., 1962.

11. Dwight, Herbert Bristol: Tables of Integrals and Other Mathematical Data. Third ed., The Macmillan Co., 1957, p. 44.

12. Bickley, W. G.: Formulae for Numerical Differentiation. The Math. Gazette, vol. 25, no. 263, Feb. 1941, p. 192.

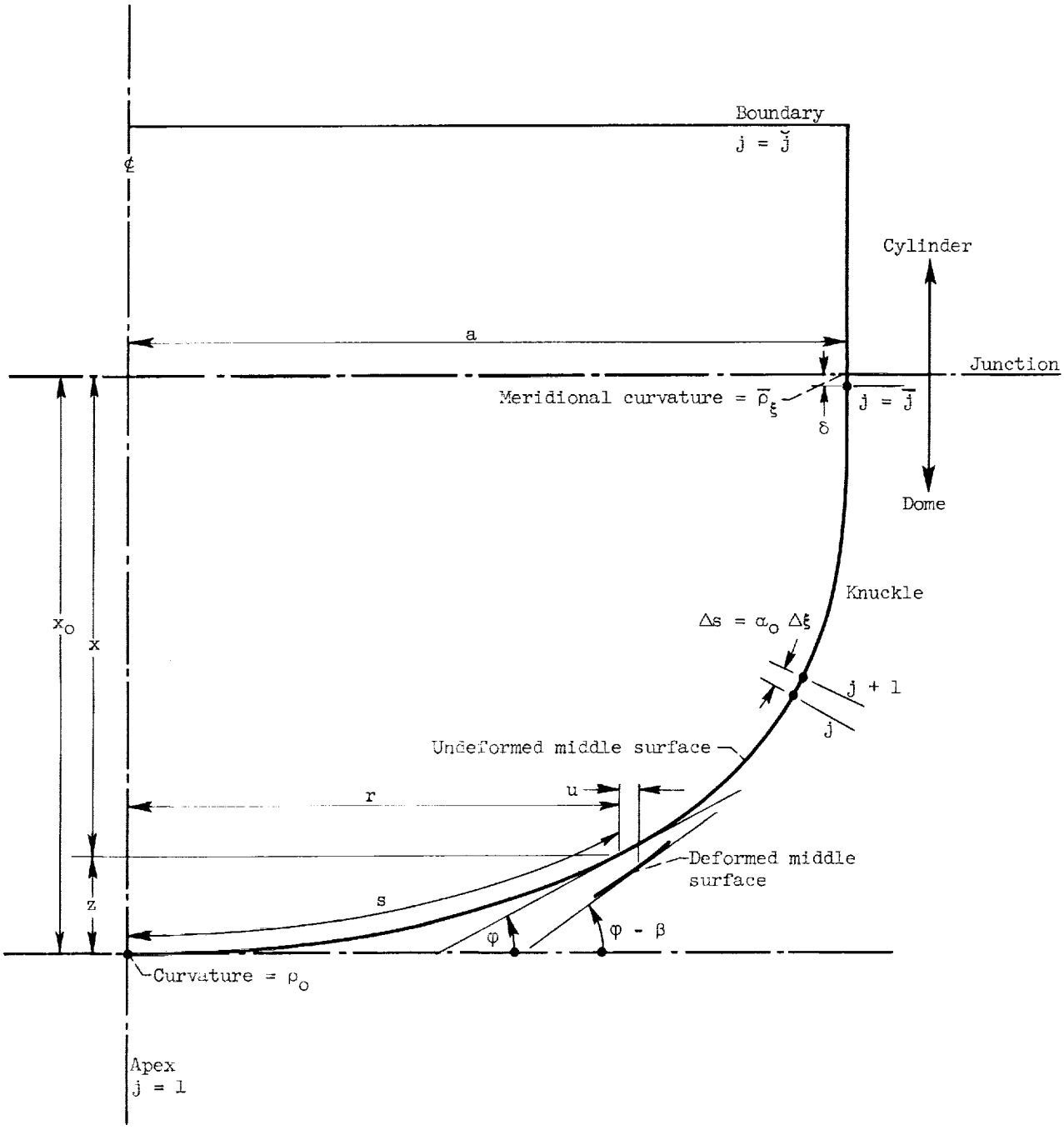

(a) Meridional geometry.

Figure 1. - Nomenclature, geometry, and sign convention.

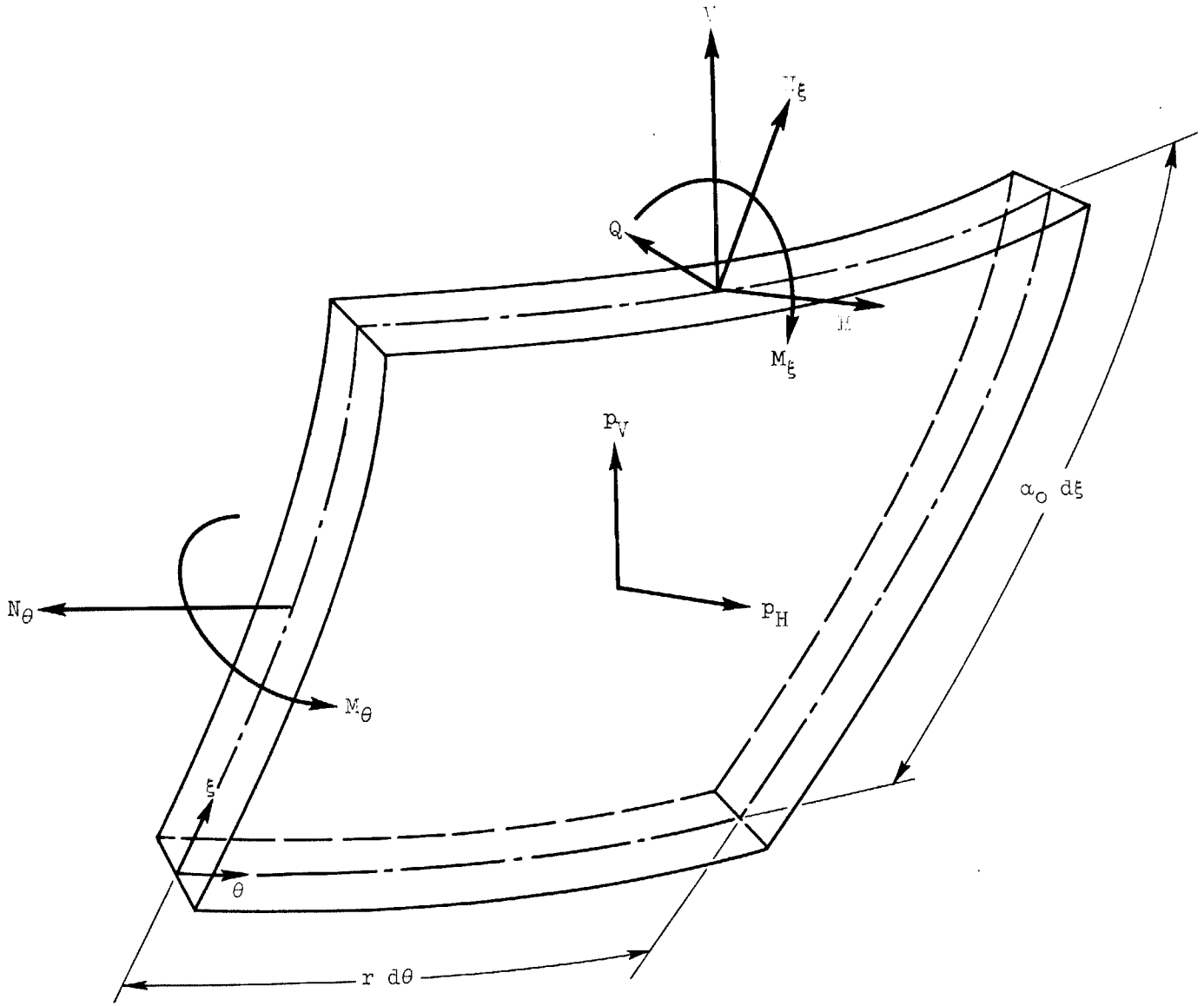

(b) Stress resultants, couples, and loads.

Figure 1. - Concluded. Nomenclature, geometry, and sign convention.

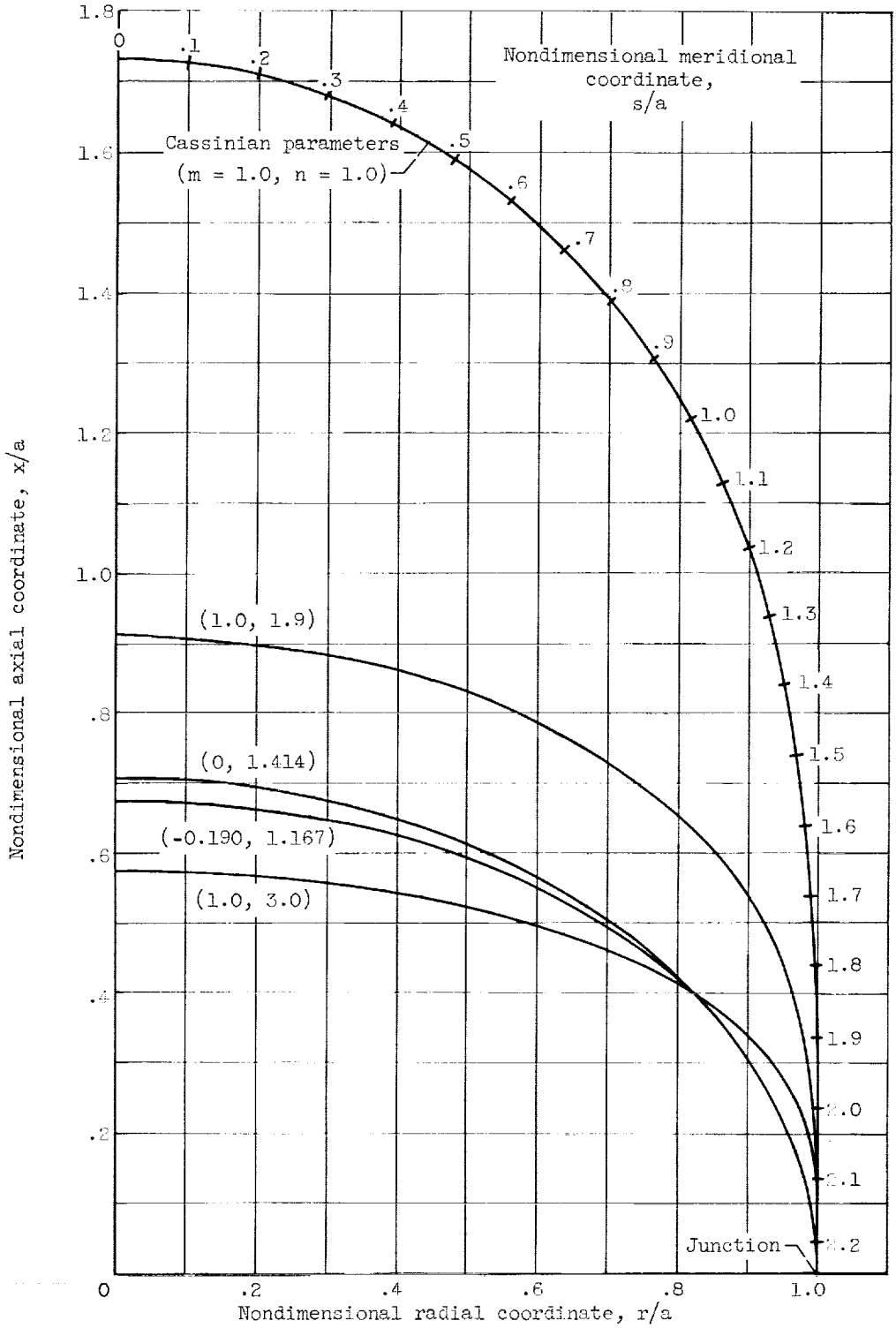

(a) Meridian shapes.

Figure 2. - Variation of Cassinian dome properties with parameters m and n.

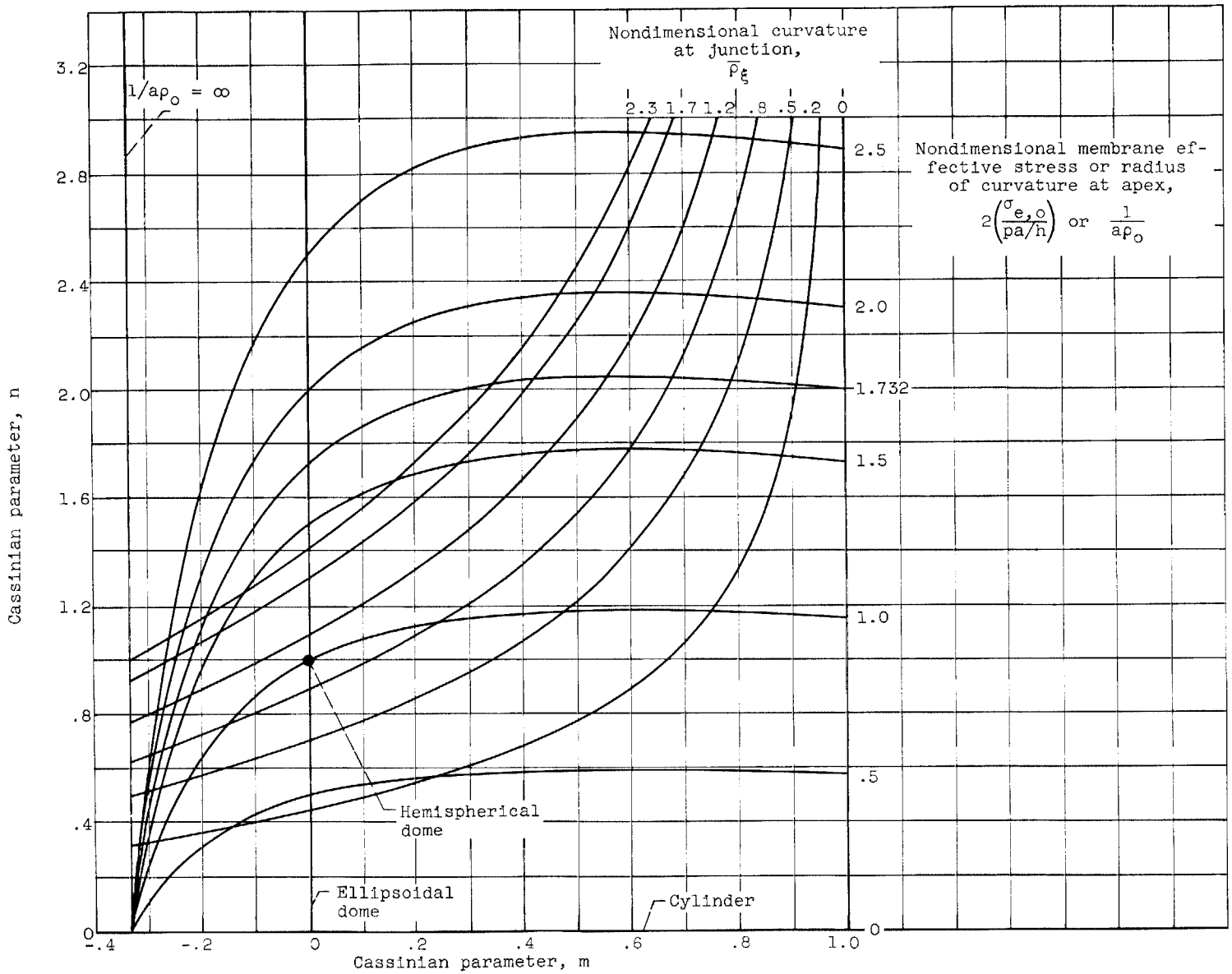

(b) Curvature at junction, apex membrane effective stress, and radius of curvature at apex.

Figure 2. - Continued. Variation of Cassinian dome properties with parameters m and n.

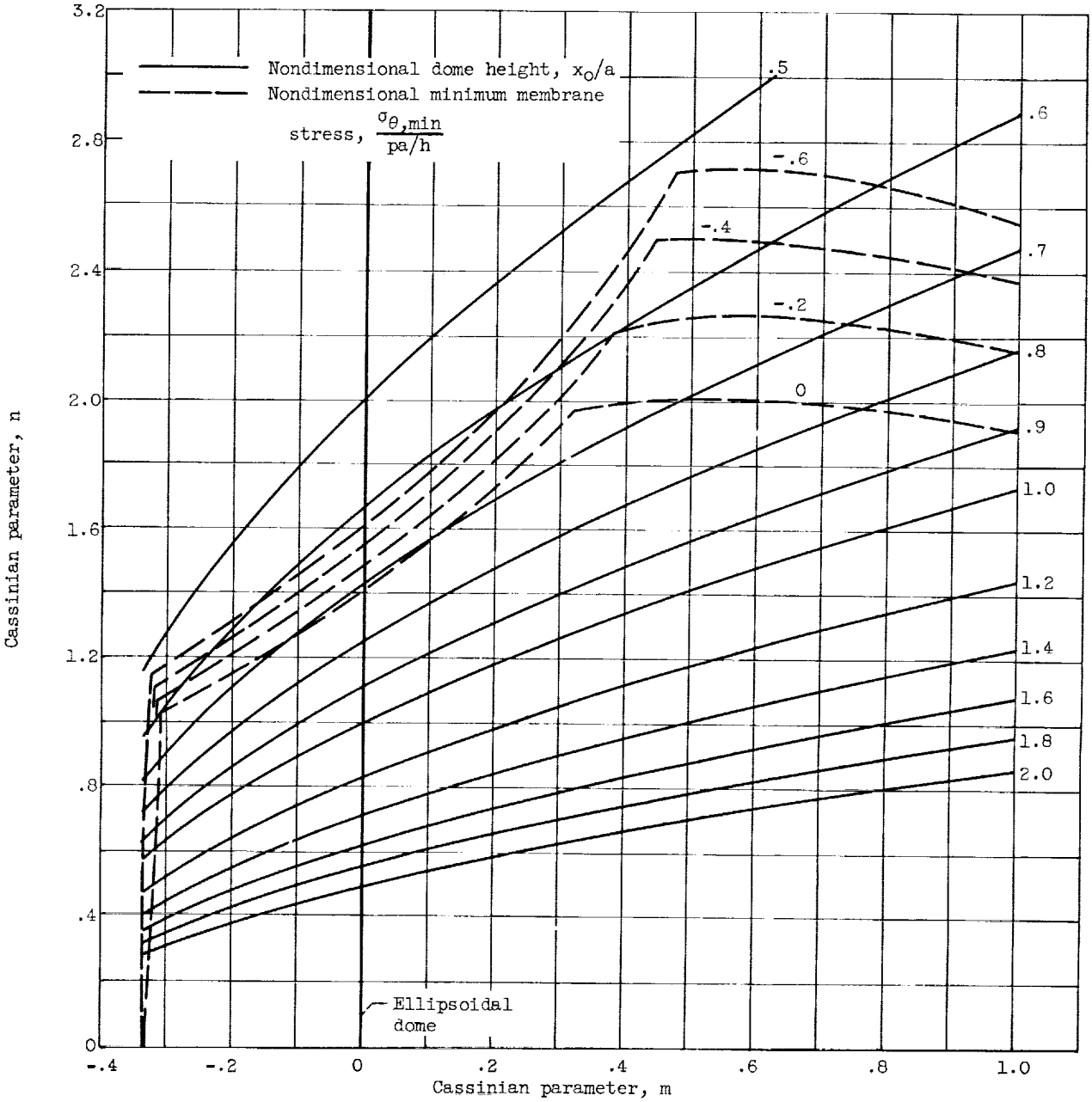

(c) Dome height and minimum membrane stress.

Figure 2. - Continued. Variation of Cassinian dome properties with parameters m and n.

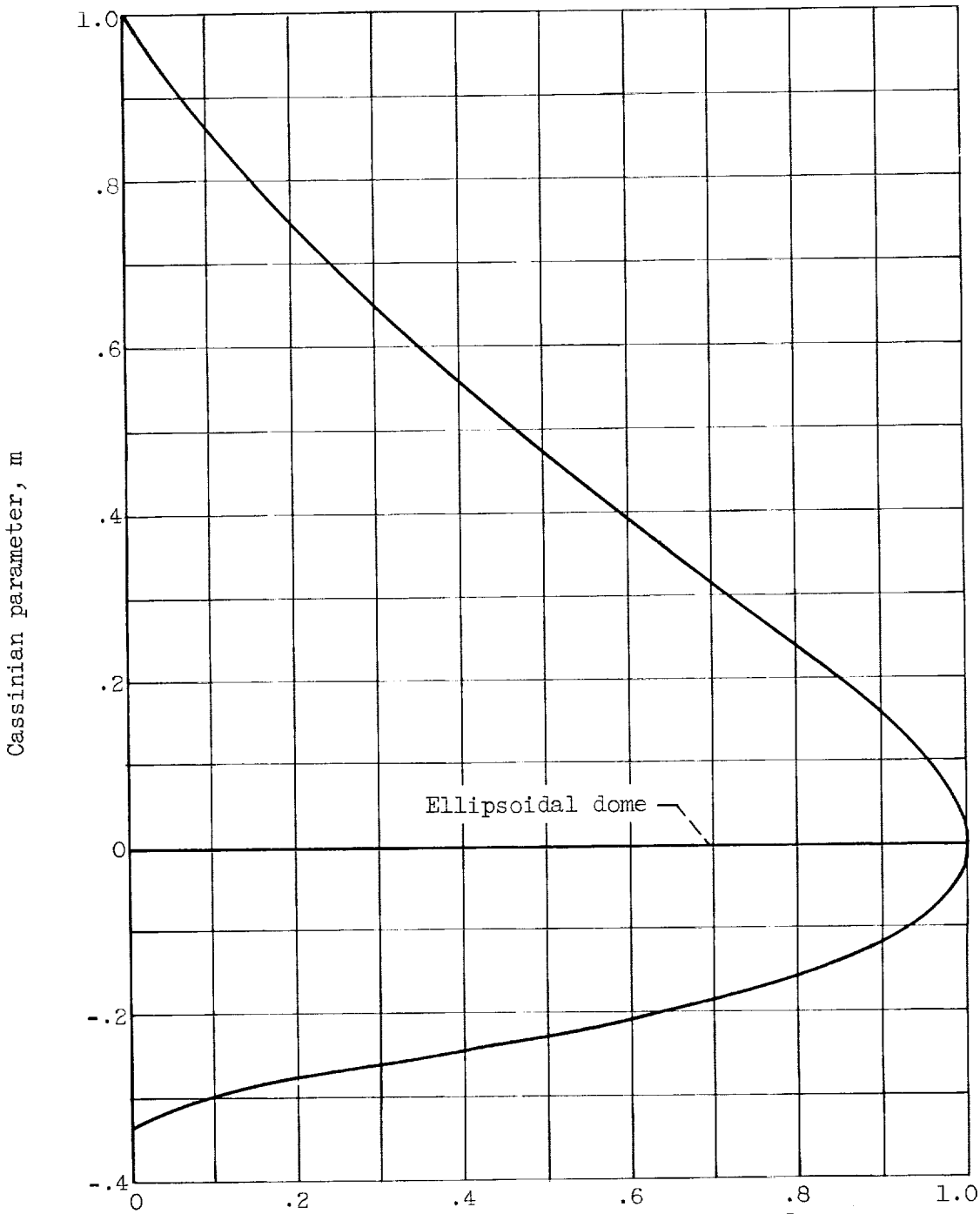

(d) Curvature constant $(a\rho_o)^2(a\bar{\rho}_\xi)$.

Figure 2. - Continued. Variation of Cassinian dome properties with parameters m and n.

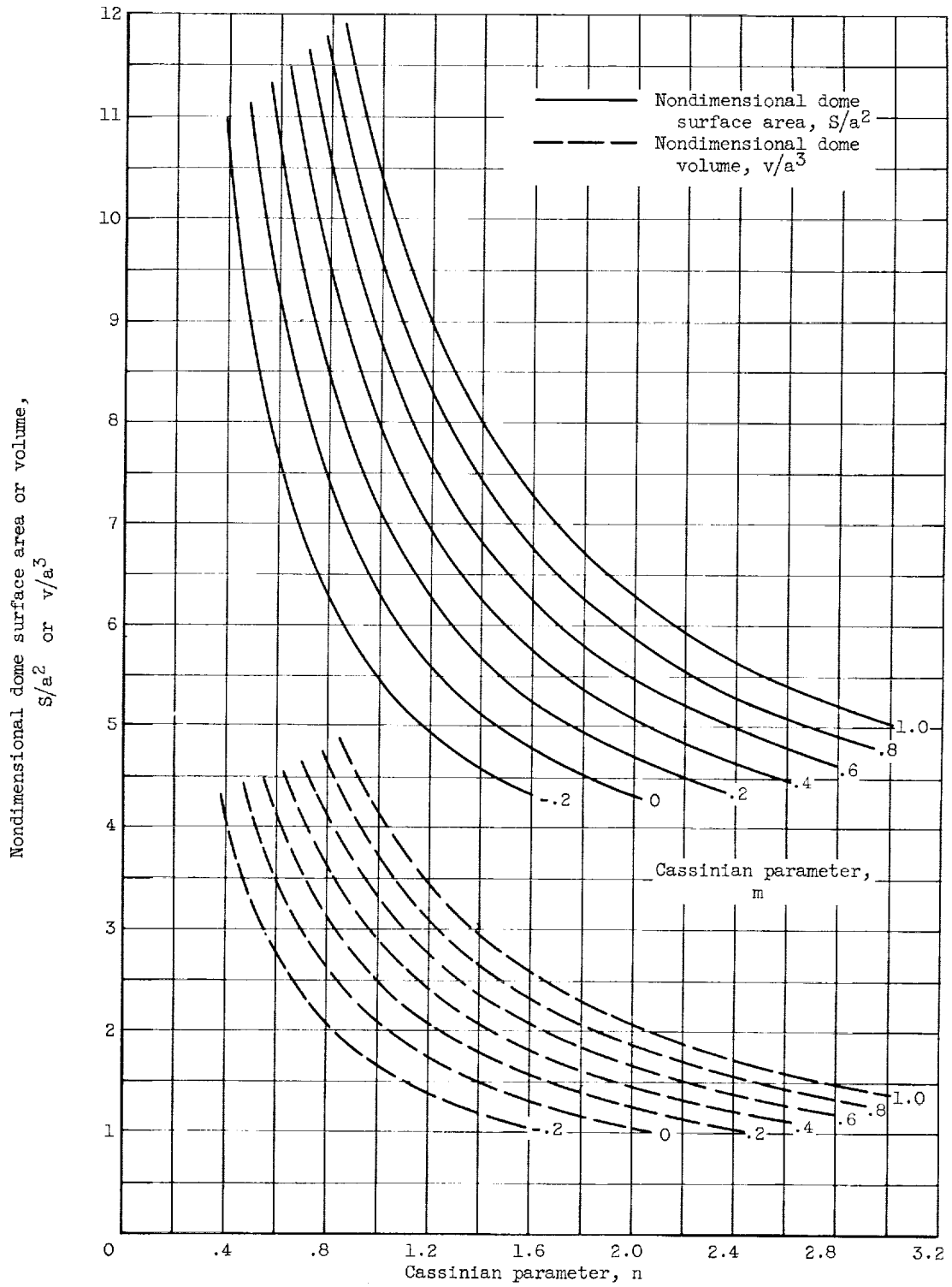

(e) Surface area and volume.

Figure 2. - Continued. Variation of Cassinian dome properties with parameters m and n.

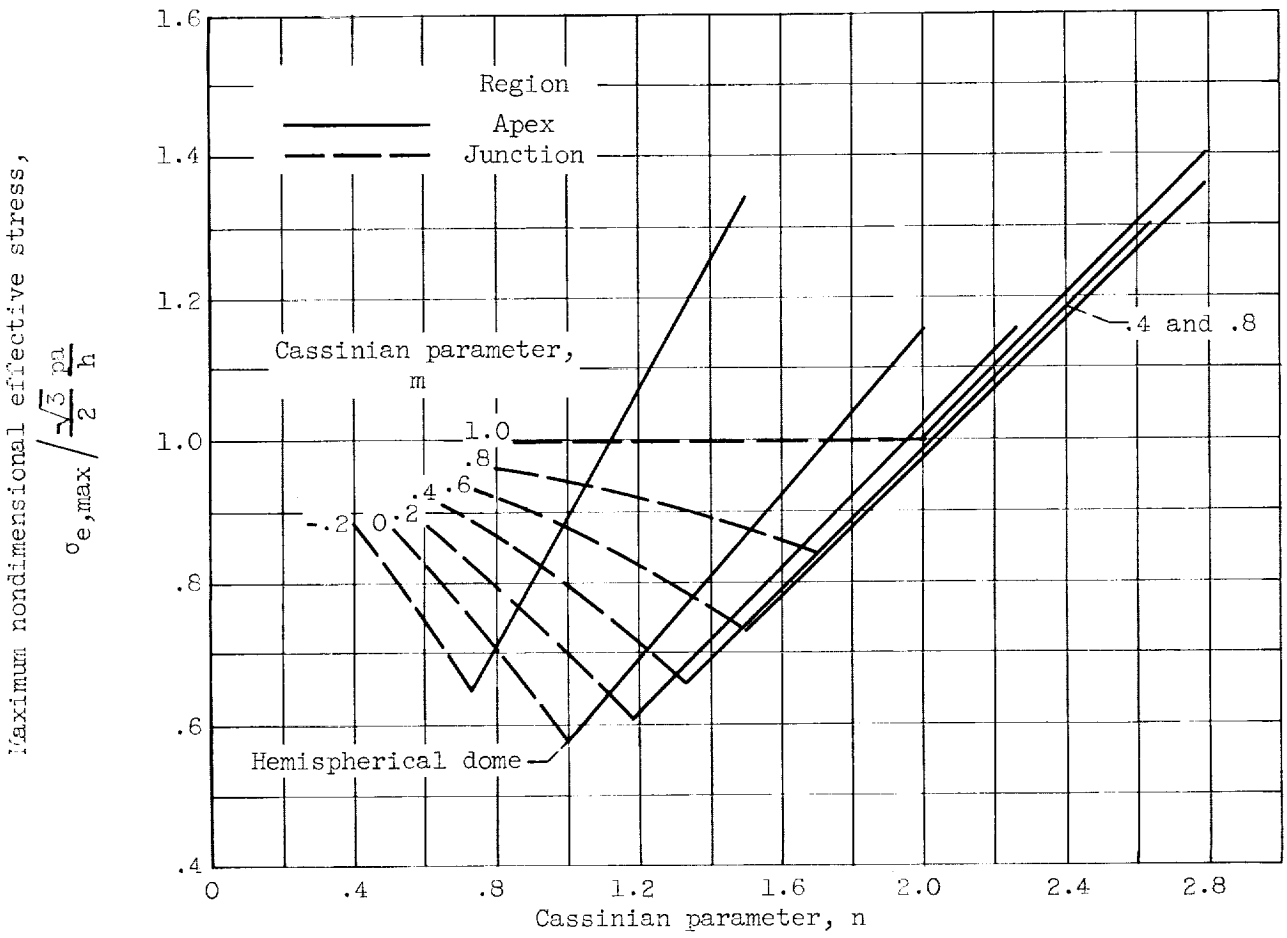

(f) Maximum effective stress.

Figure 2. - Concluded. Variation of Cassinian dome properties with parameters m and n.

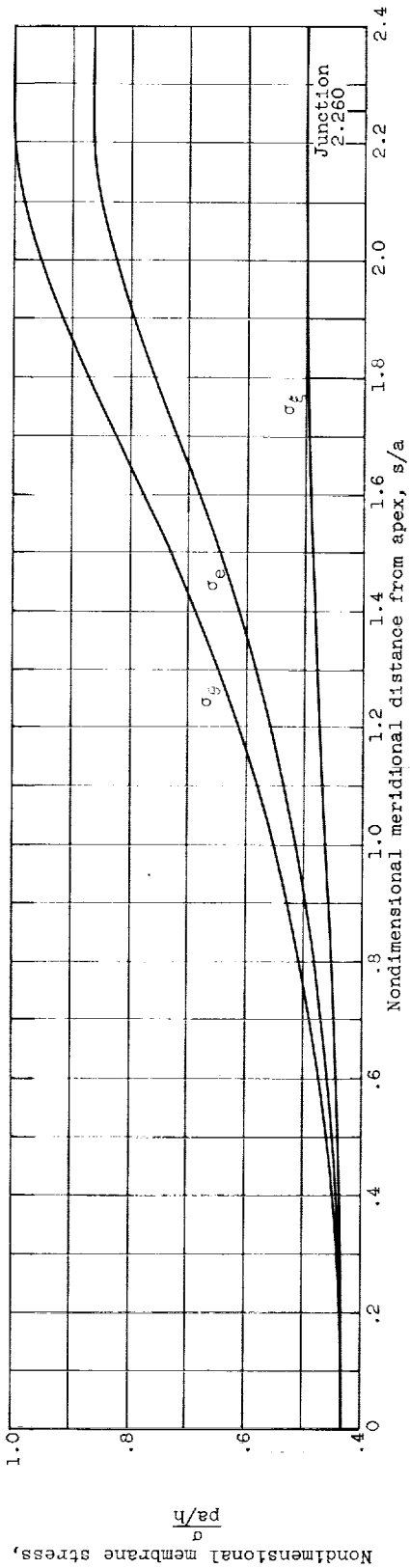

(a) Cassinian parameter n, 1.0.

Figure 3. - Membrane stresses in Cassinian domes with zero junction curvature (m = 1.0).

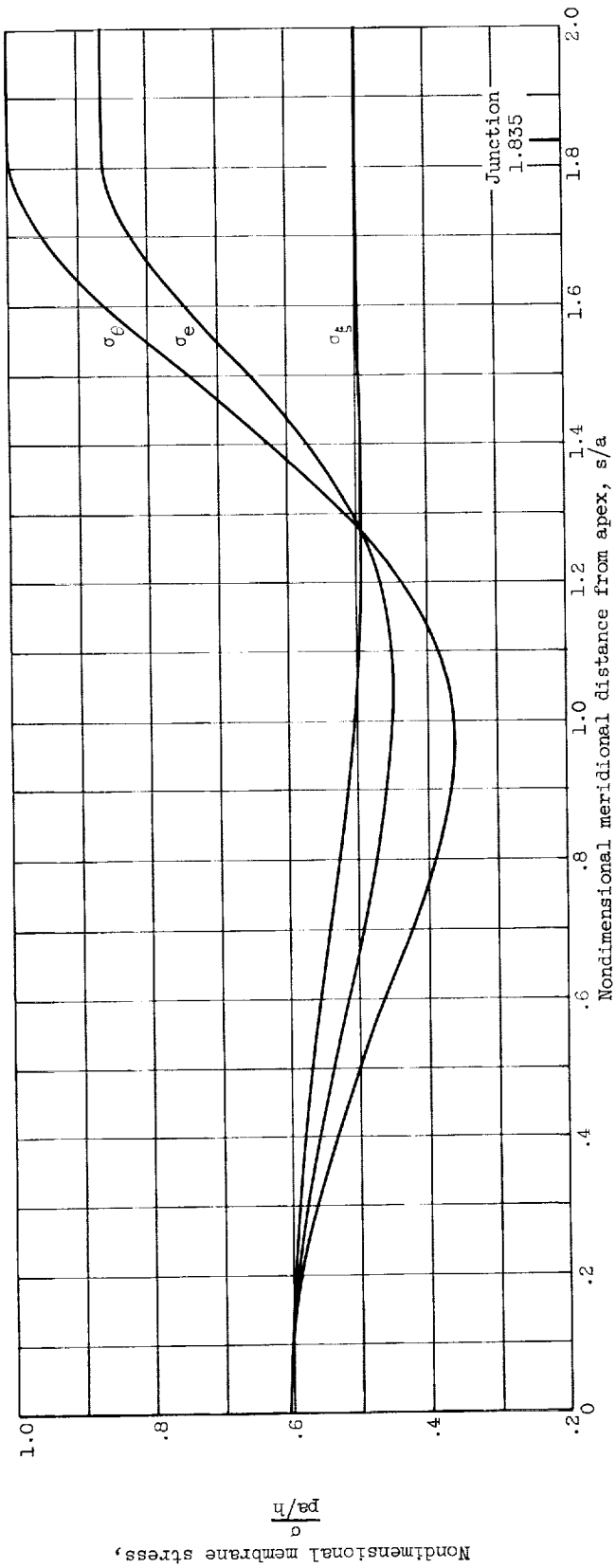

(b) Cassinian parameter n, 1.4.

Figure 3. - Continued. Membrane stresses in Cassinian domes with zero junction curvature (m = 1.0).

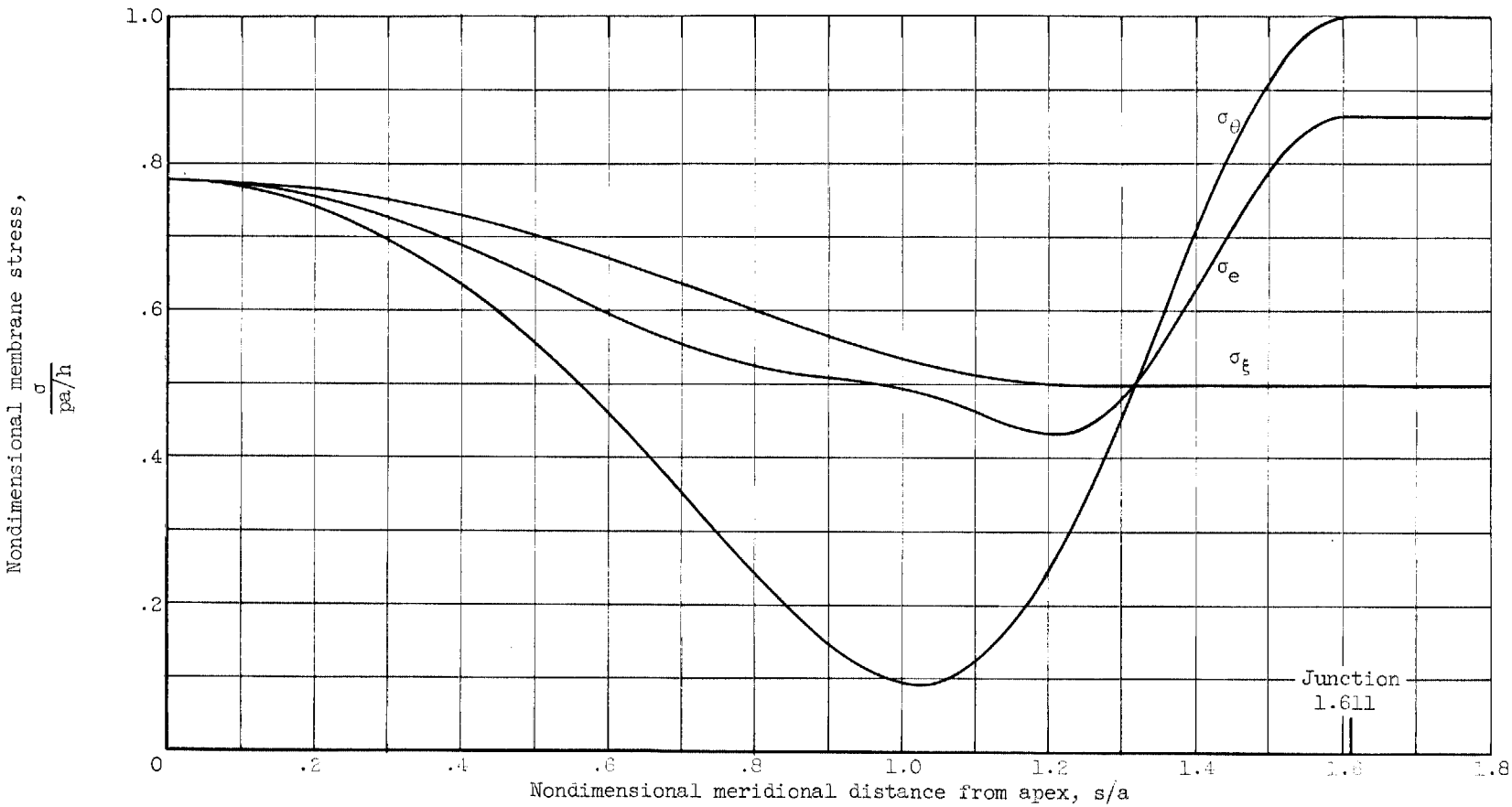

(c) Cassinian parameter n, 1.8.

Figure 3. - Continued. Membrane stresses in Cassinian domes with zero junction curvature (m = 1.0).

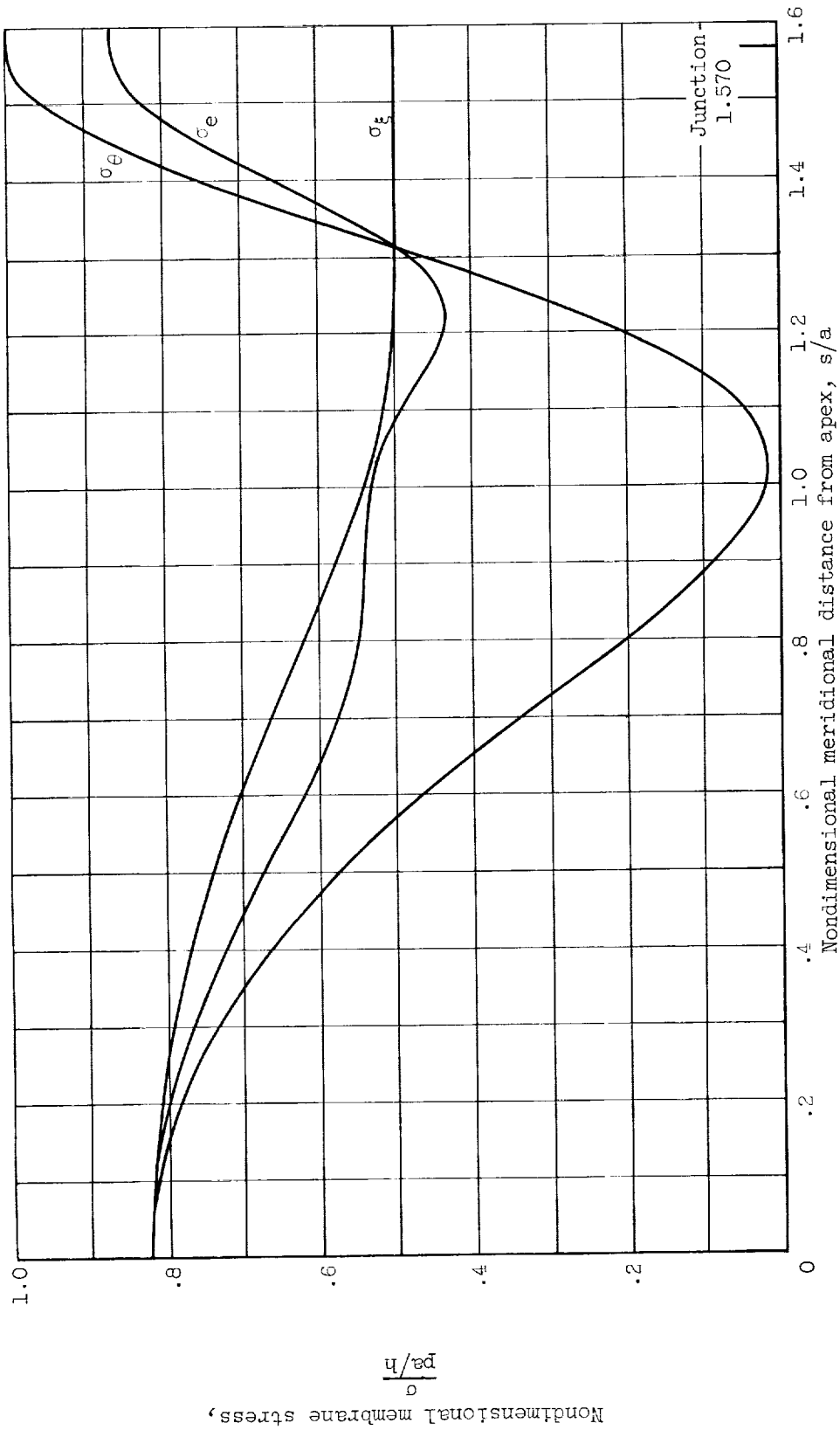

(d) Cassinian parameter n, 1.9.

Figure 3. - Continued. Membrane stresses in Cassinian domes with zero junction curvature (m = 1.0).

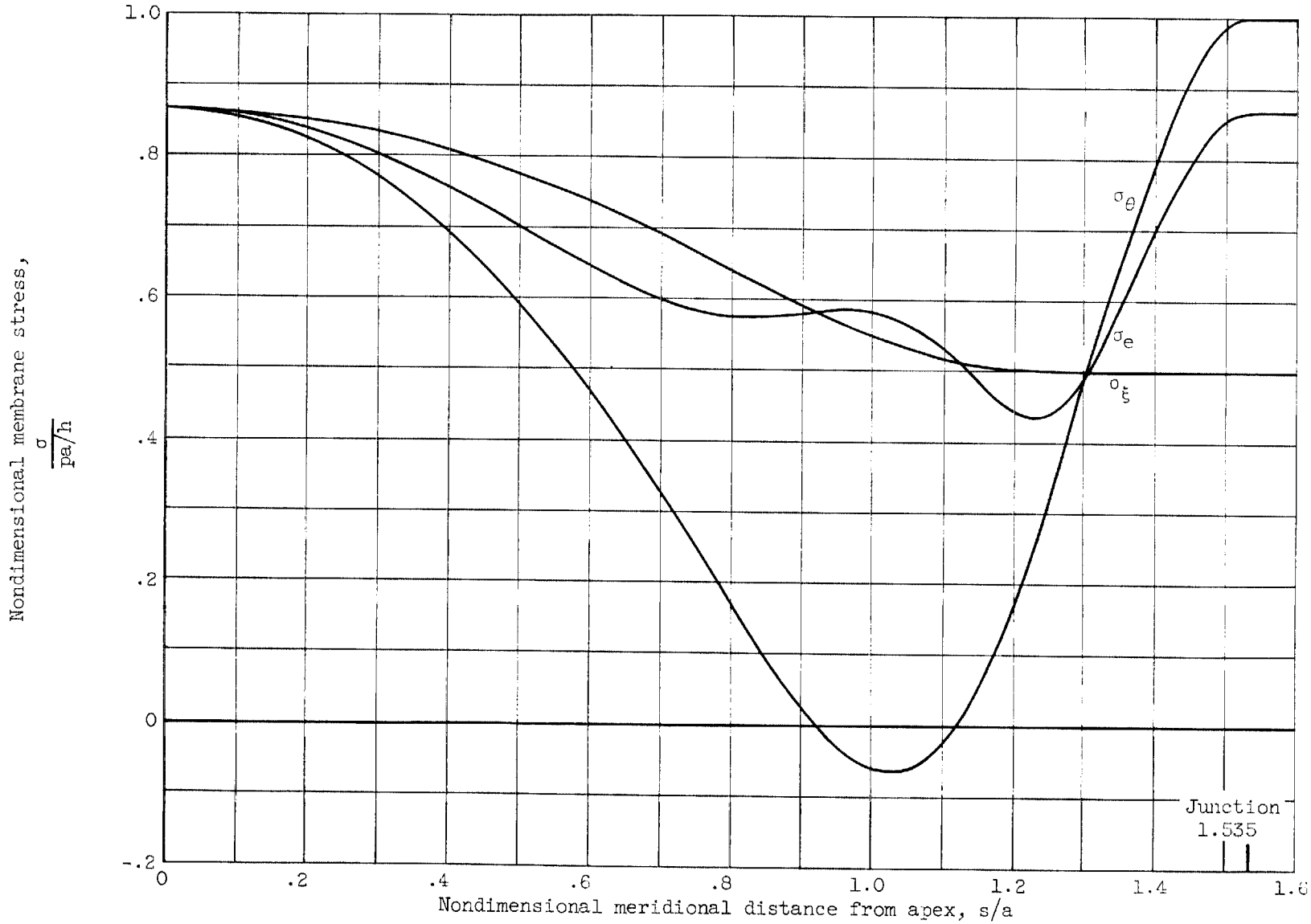

(e) Cassinian parameter n, 2.0.

Figure 3. - Continued. Membrane stresses in Cassinian domes with zero junction curvature (m = 1.0).

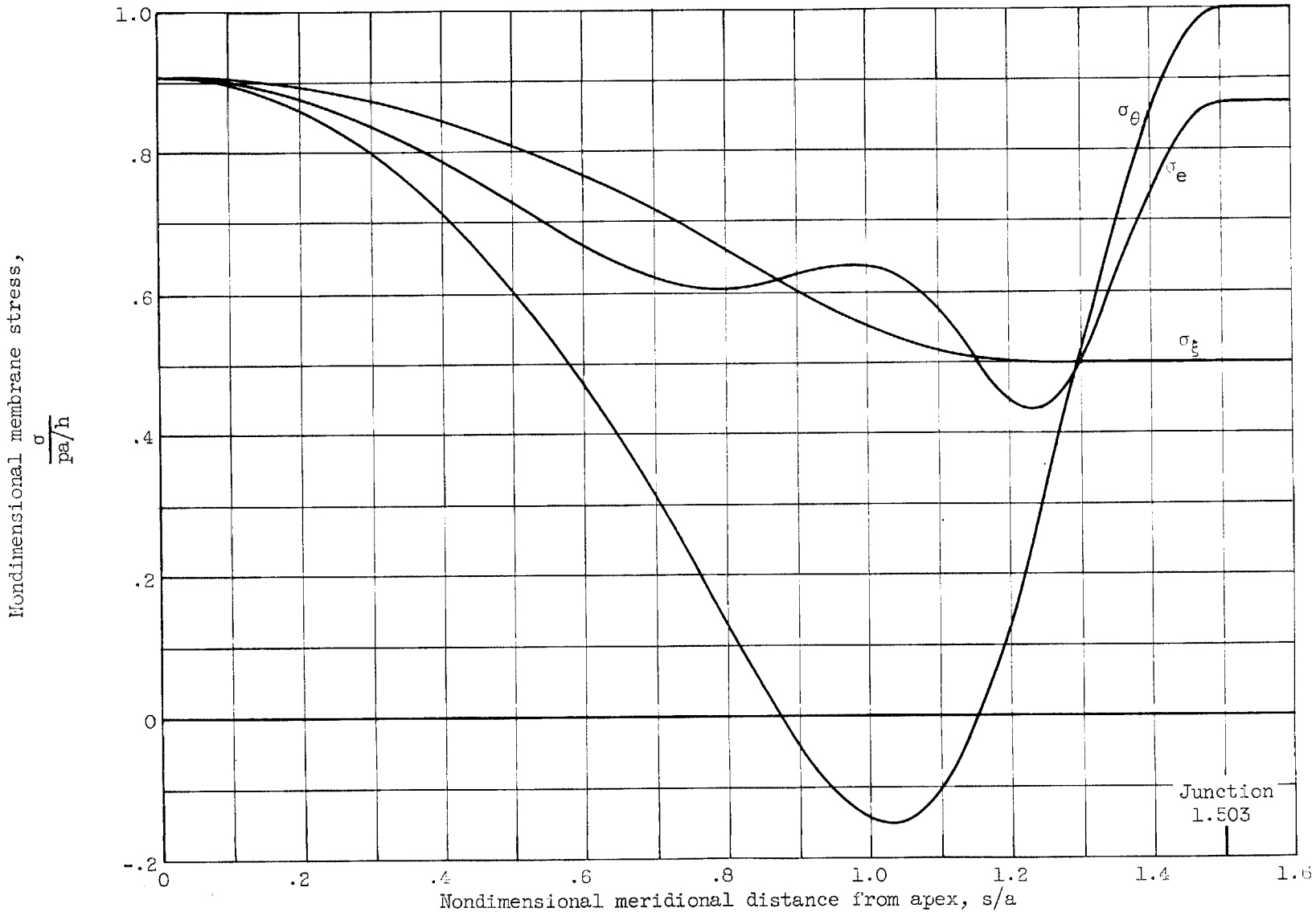

(f) Cassinian parameter n, 2.1.

Figure 3. - Continued. Membrane stresses in Cassinian domes with zero junction curvature (m = 1.0).

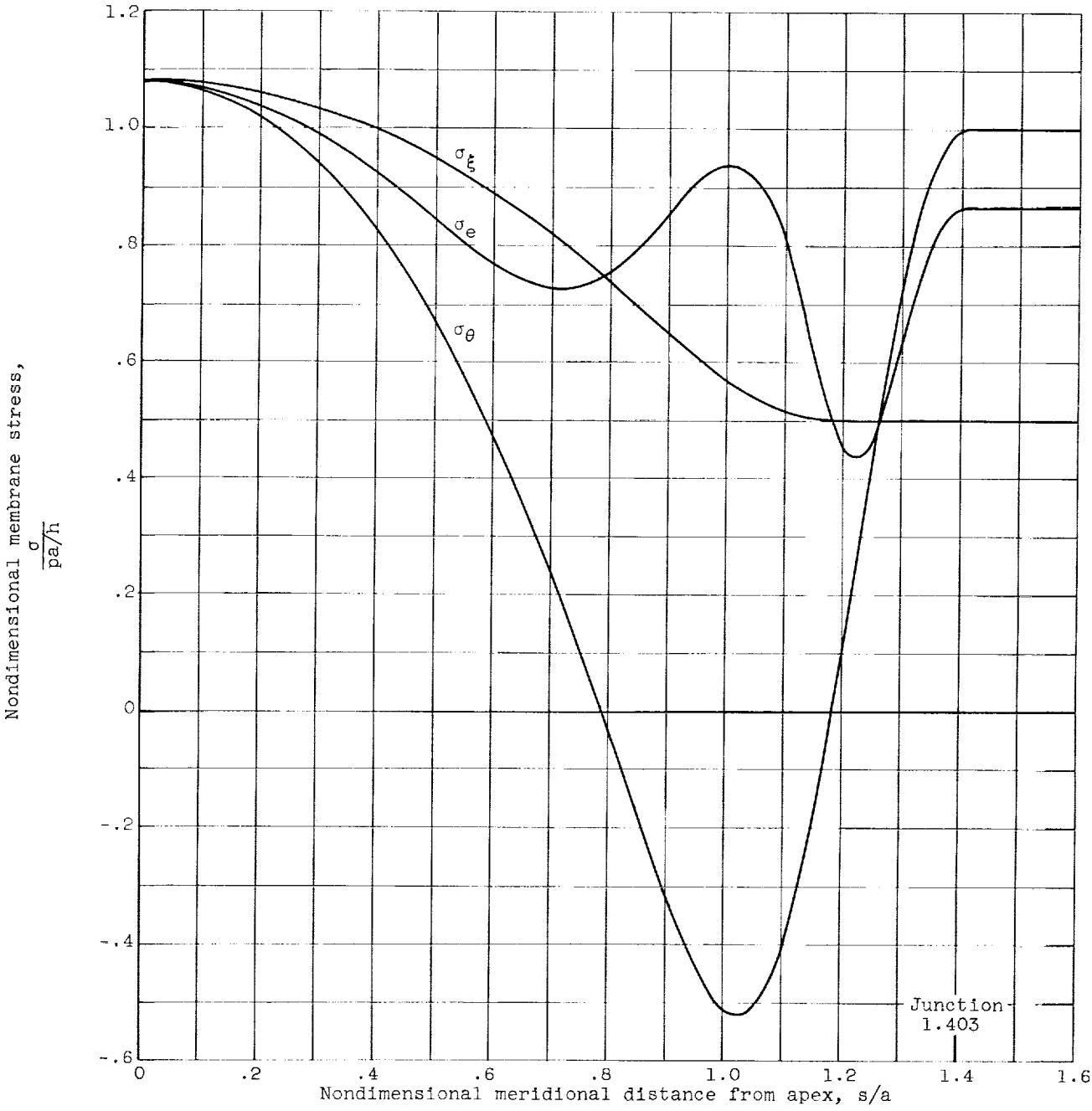

(g) Cassinian parameter n, 2.5.

Figure 3. - Continued. Membrane stresses in Cassinian domes with zero junction curvature (m = 1.0).

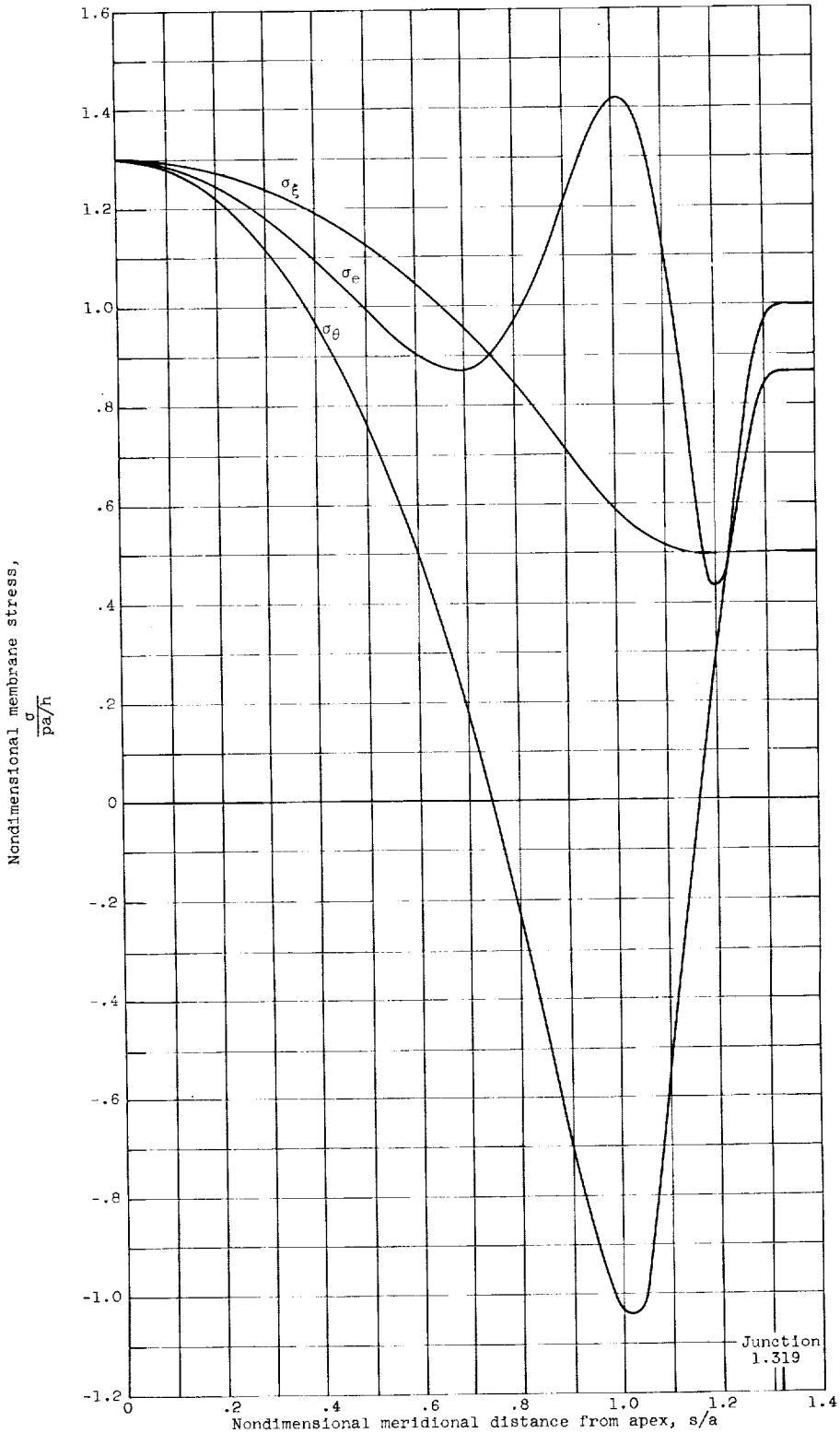

(h) Cassinian parameter n, 3.0.

Figure 3. - Concluded. Membrane stresses in Cassinian domes with zero junction curvature (m = 1.0).

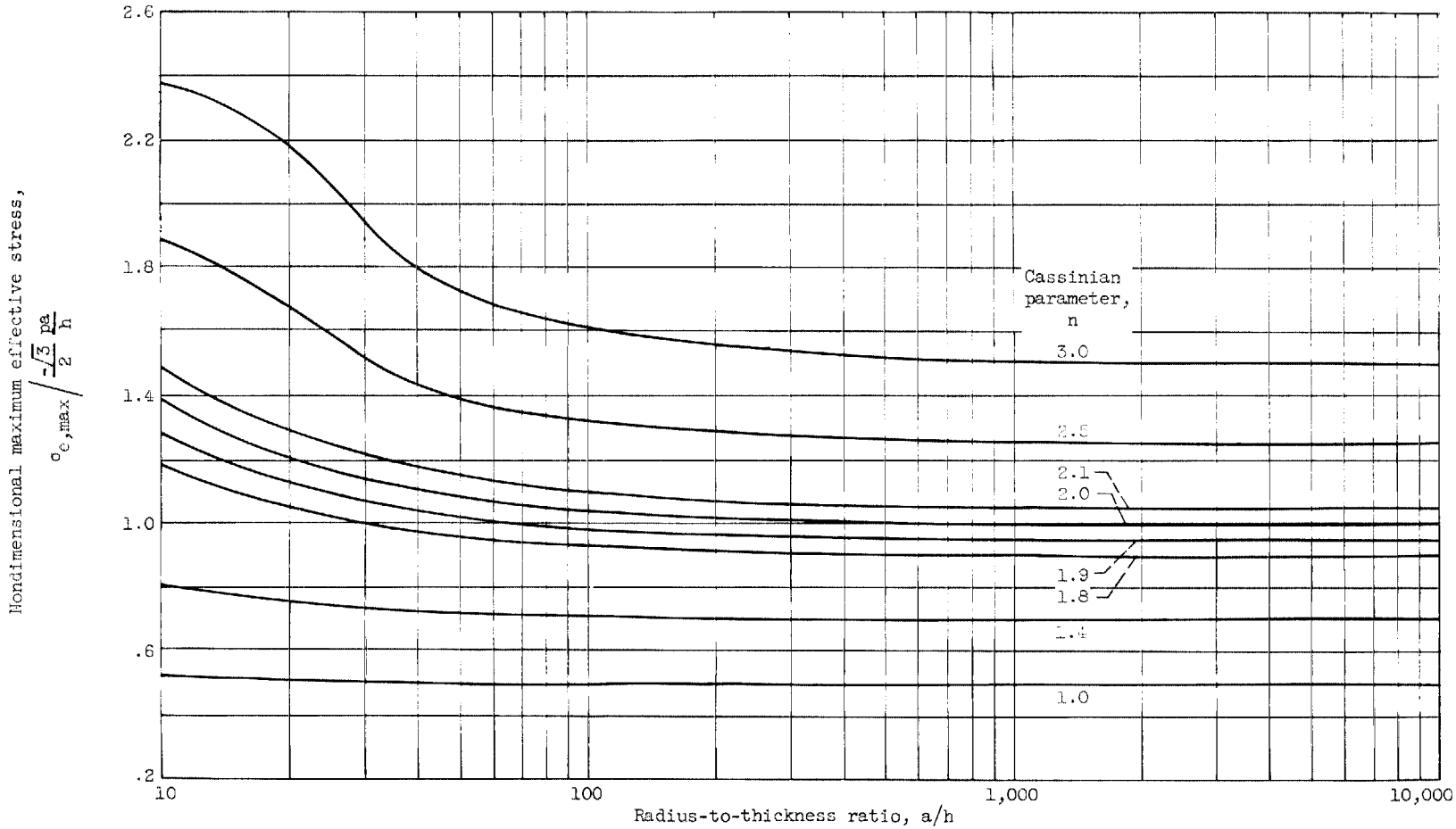

(a) Apex.

Figure 4. - Relative maximum effective stress as a function of radius-to-thickness ratio in Cassinian domes with zero junction curvature. Cassinian parameter m, 1.0; Poisson's ratio, 0.3.

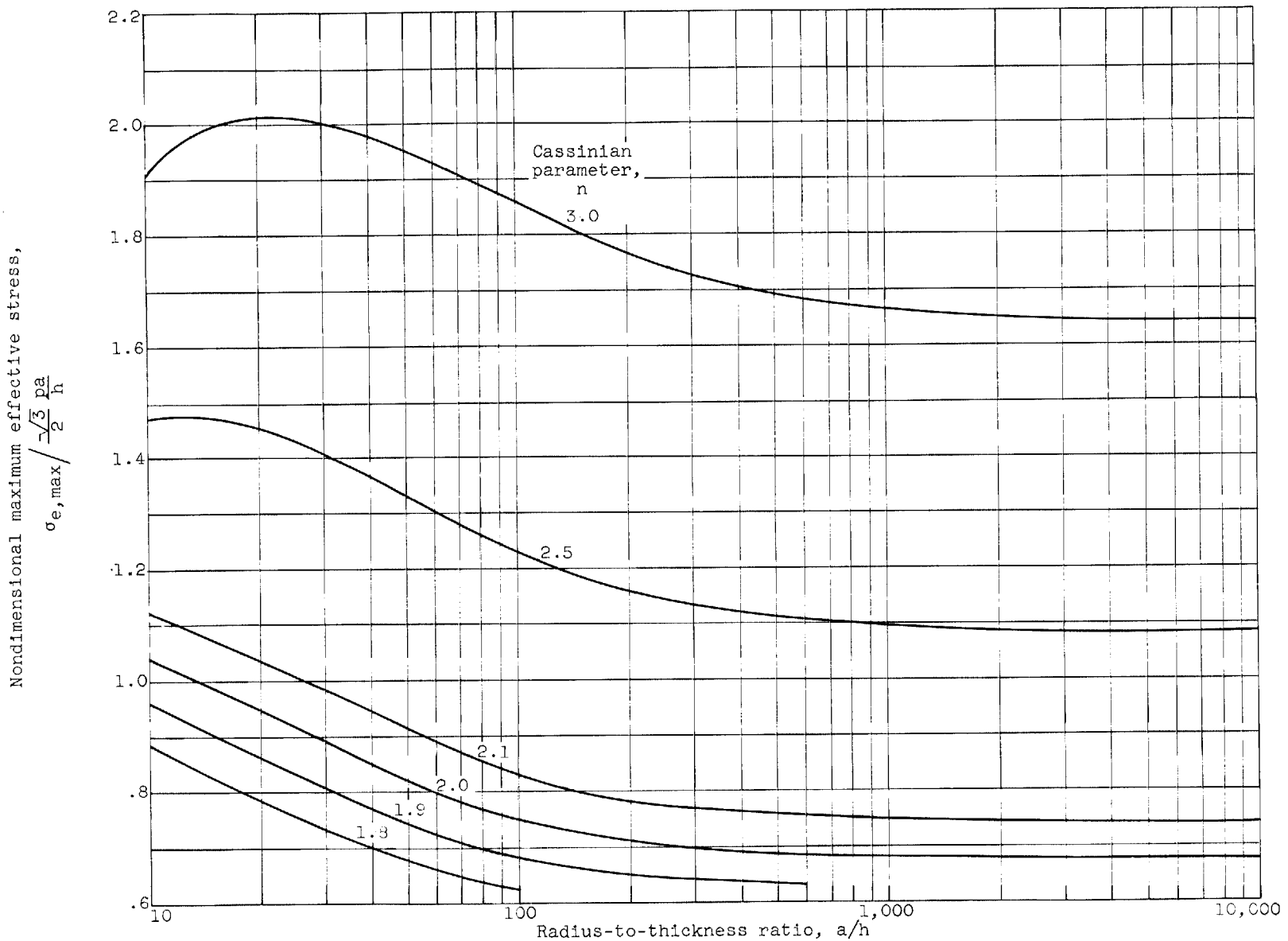

(b) Region of knuckle.

Figure 4. - Continued. Relative maximum effective stress as a function of radius-to-thickness ratio in Cassinian domes with zero junction curvature. Cassinian parameter m, 1.0; Poisson's ratio, 0.3.

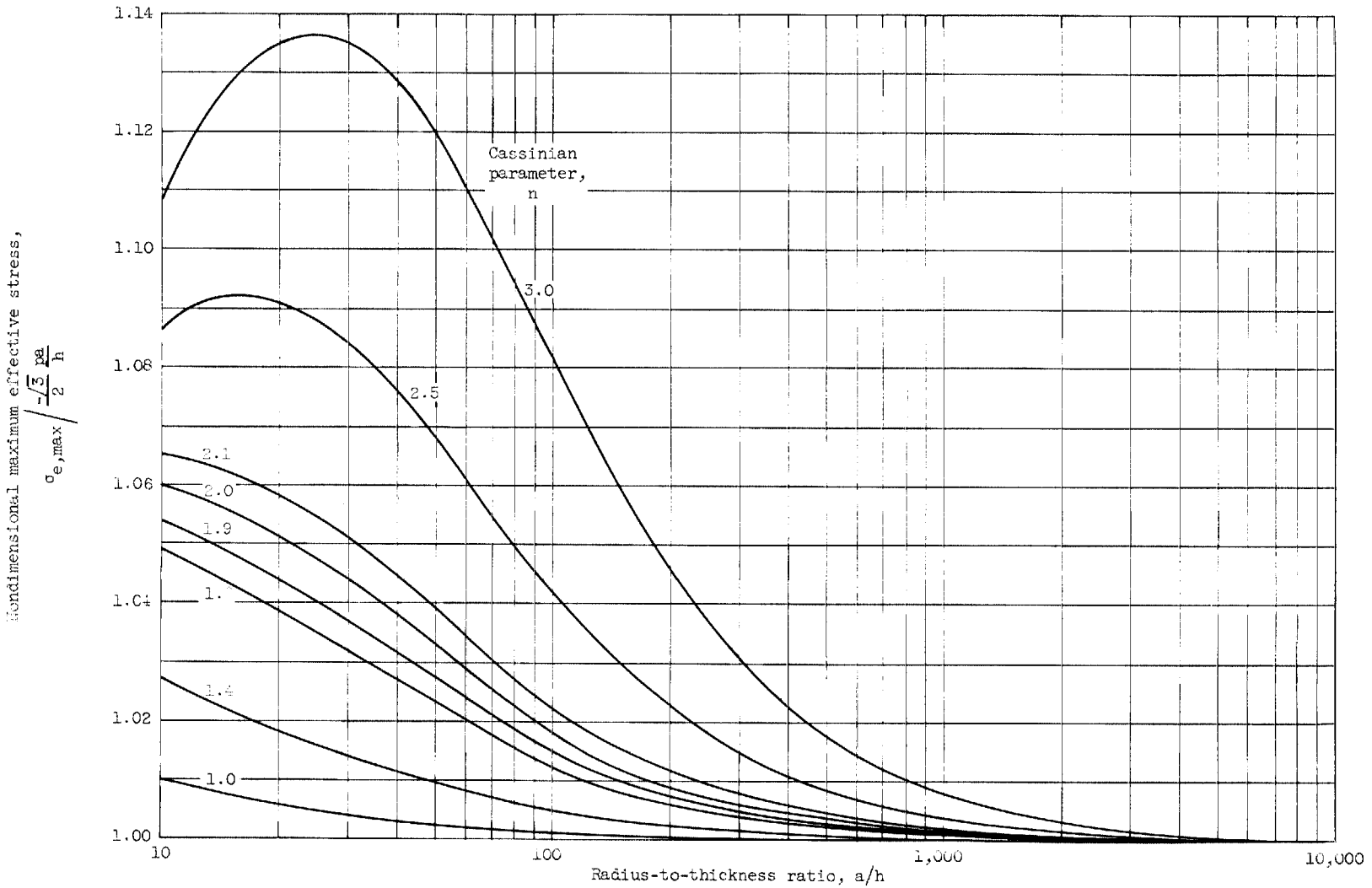

(c) Region of junction.

Figure 4. - Continued. Relative maximum effective stress as a function of radius-to-thickness ratio in Cassinian domes with zero junction curvature. Cassinian parameter m, 1.0; Poisson's ratio, 0.3.

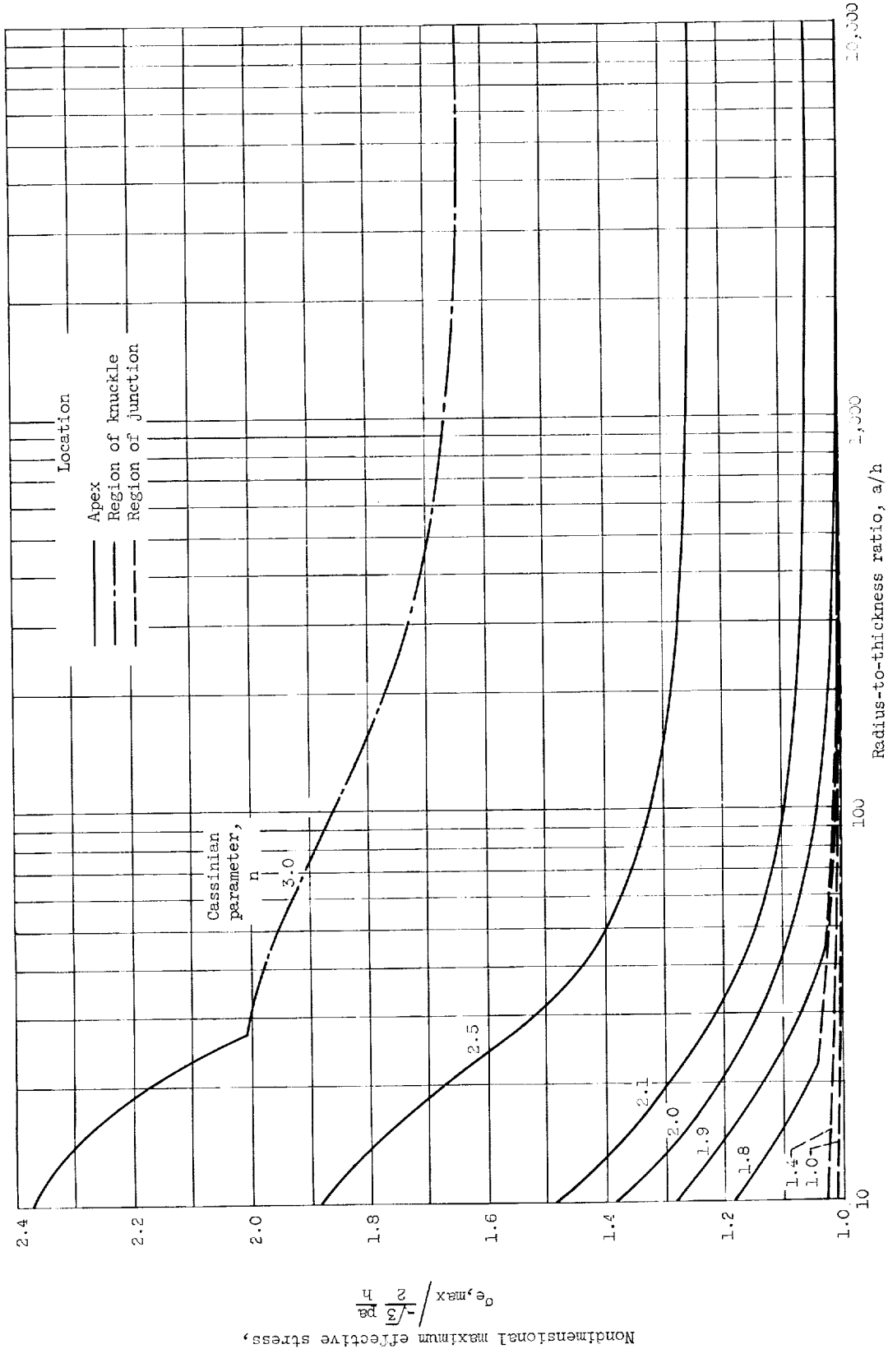

(d) Critical region.

Figure 4. - Concluded. Relative maximum effective stress as a function of radius-to-thickness ratio in Cassinian domes with zero junction curvature. Cassinian parameter m, 1.0; Poisson's ratio, 0.3.

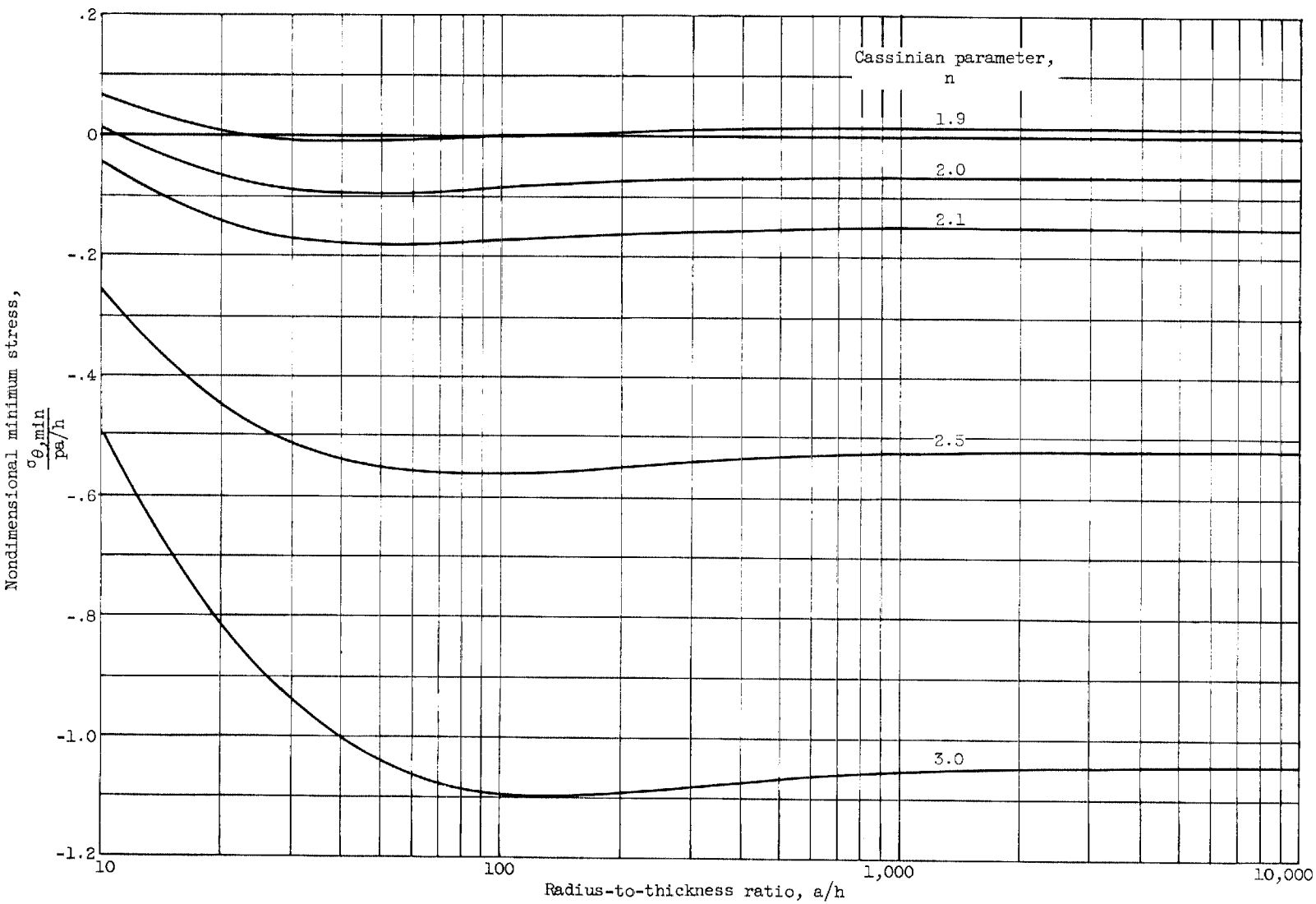

Figure 5. - Minimum stress as a function of radius-to-thickness ratio in Cassinian domes with zero junction curvature. Cassinian parameter m, 1.0; Poisson's ratio, 0.3.

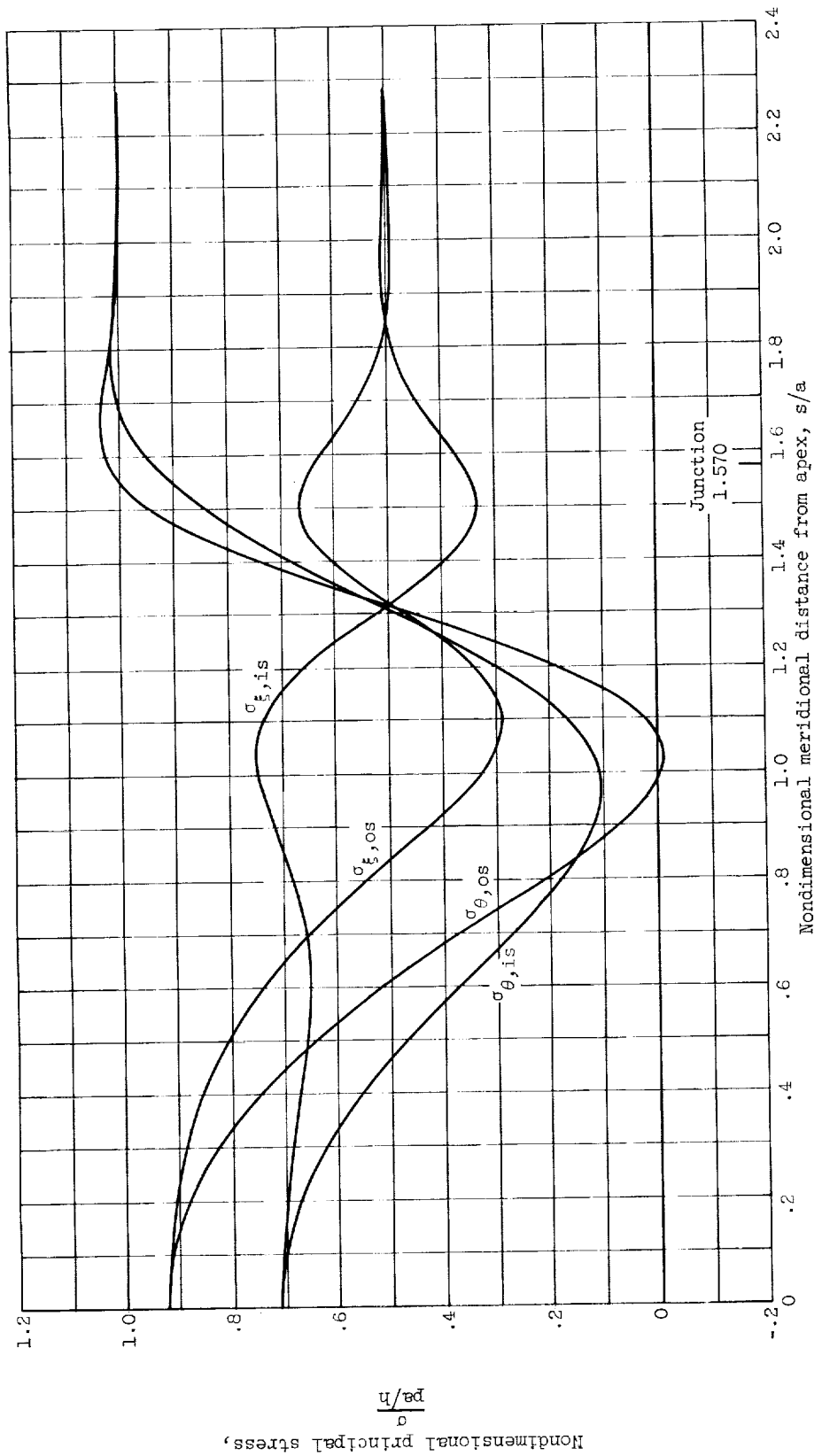

(a) Radius-to-thickness ratio, 30.

Figure 6. - Principal stresses as a function of meridional distance from apex. Cassinian parameter m, 1.0; Cassinian parameter n, 1.9; Poisson's ratio, 0.3.

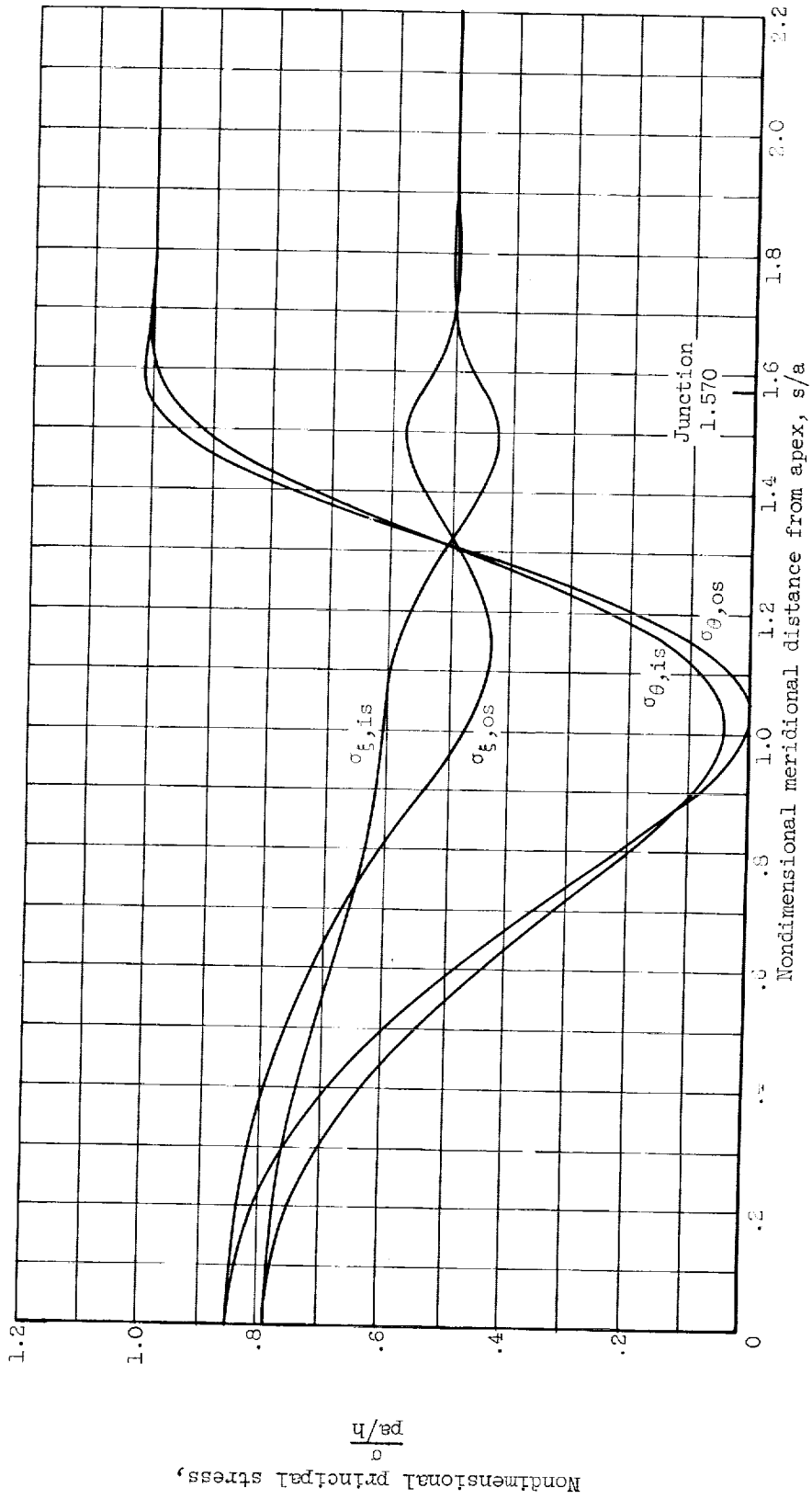

(b) Radius-to-thickness ratio, 100.

Figure 6. - Continued. Principal stresses as a function of meridional distance from apex. Cassinian parameter m, 1.0; Cassinian parameter n, 1.3; Poisson's ratio, 0.3.

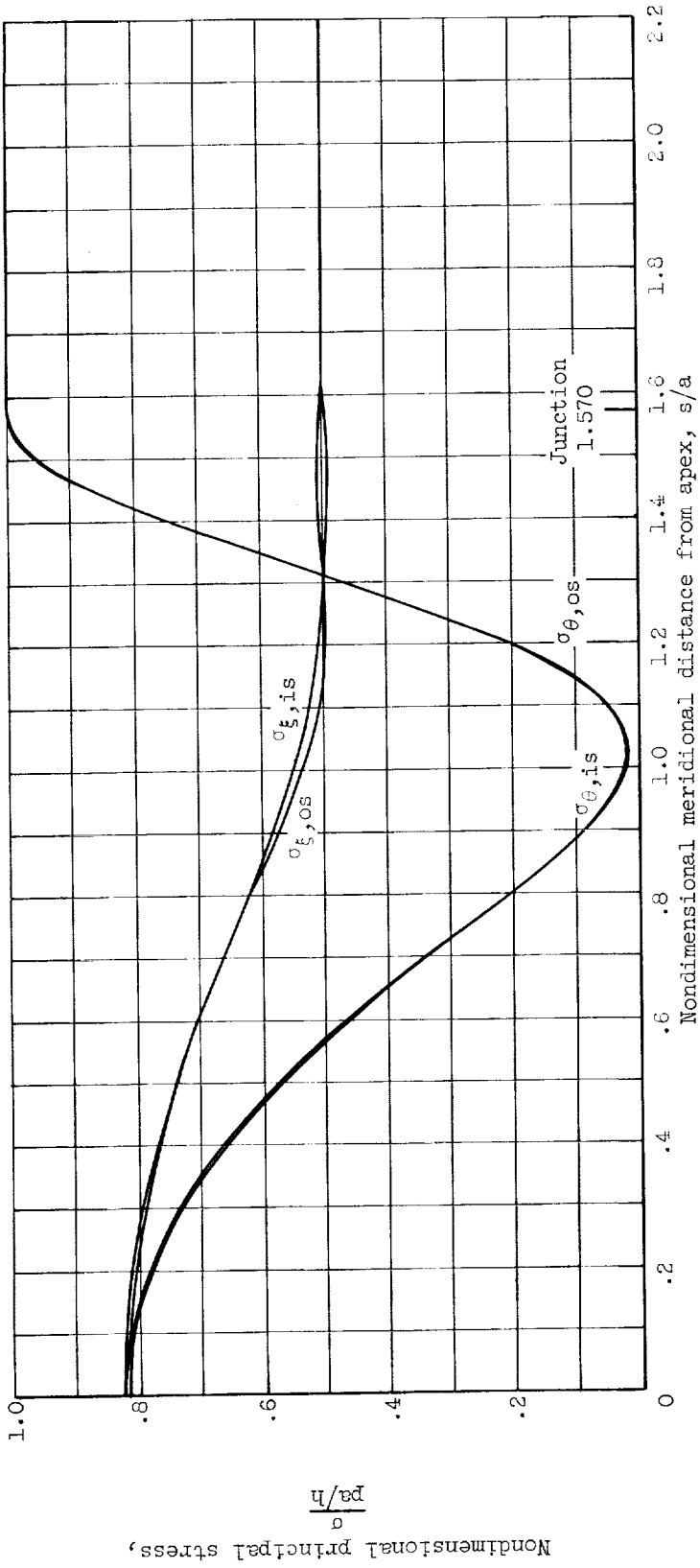

(c) Radius-to-thickness ratio, 1000.

Figure 6. - Concluded. Principal stresses as a function of meridional distance from apex. Cassinian parameter m, 1.0; Cassinian parameter n, 1.9; Poisson's ratio, 0.3.

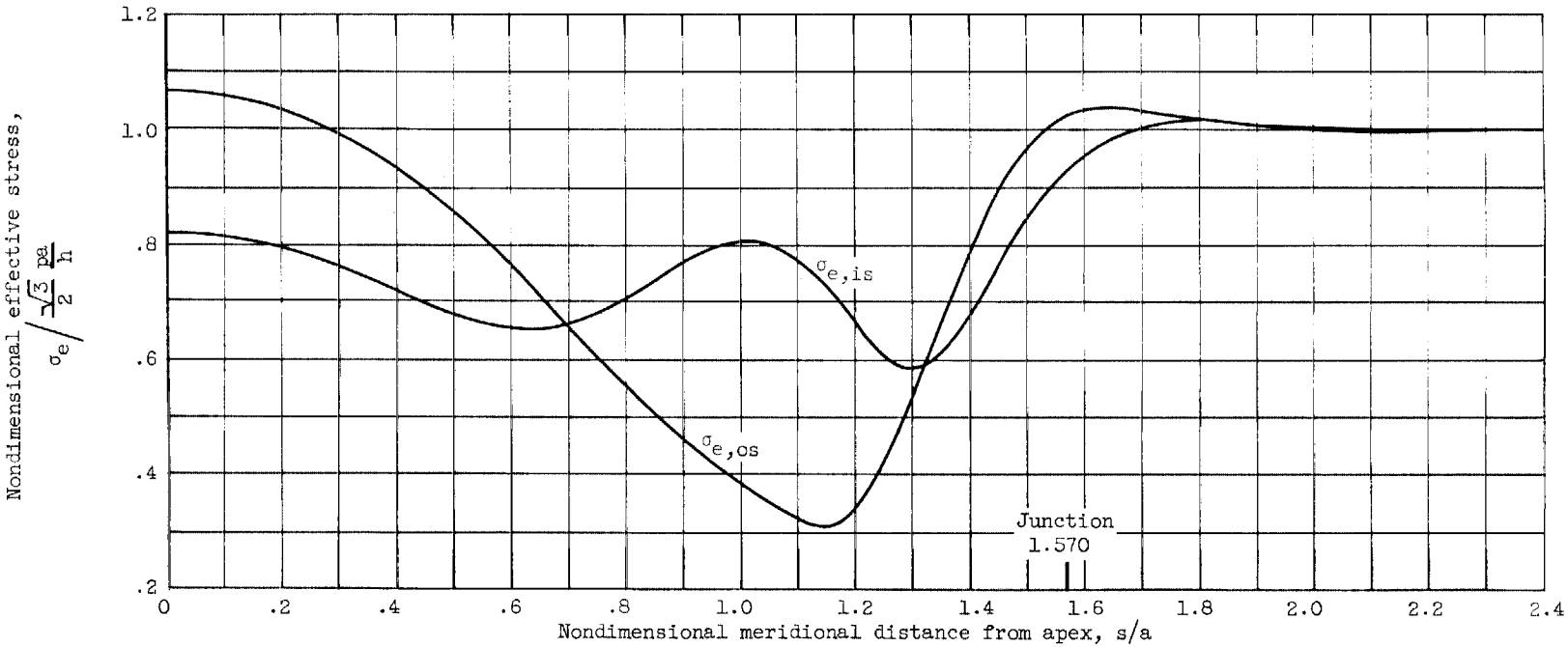

(a) Radius-to-thickness ratio, 30.

Figure 7. - Effective stresses as a function of meridional distance from apex. Cassinian parameter m, 1.0; Cassinian parameter n, 1.9; Poisson's ratio, 0.3.

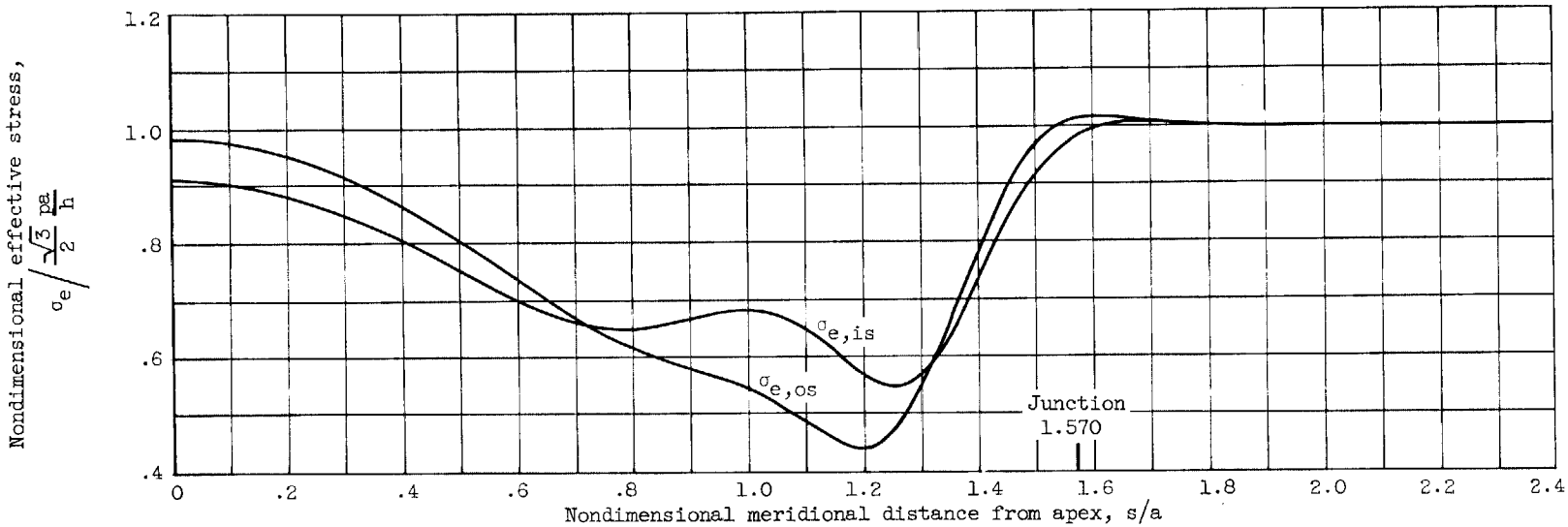

(b) Radius-to-thickness ratio, 100.

Figure 7. - Continued. Effective stresses as a function of meridional distance from apex. Cassinian parameter m, 1.0; Cassinian parameter n, 1.9; Poisson's ratio, 0.3.

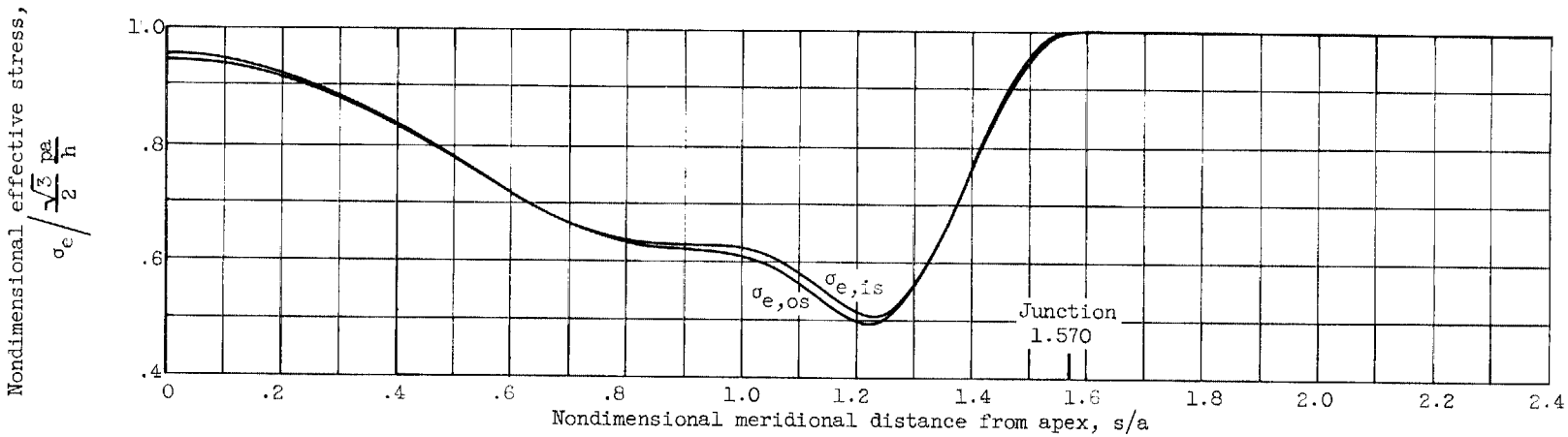

(c) Radius-to-thickness ratio, 1000.

Figure 7. - Concluded. Effective stresses as a function of meridional distance from apex. Cassinian parameter m, 1.0; Cassinian parameter n, 1.9; Poisson's ratio, 0.3.

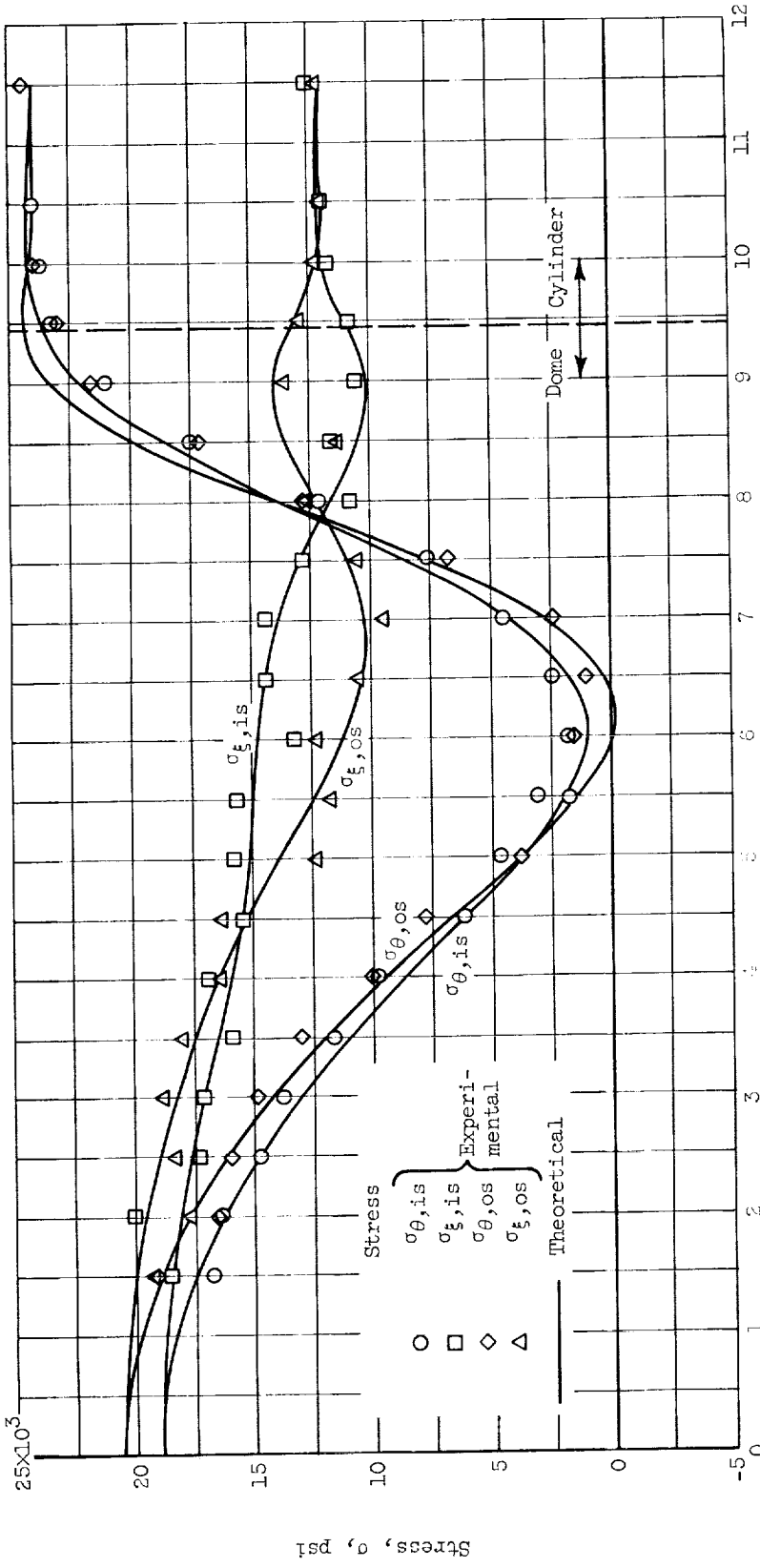

Figure 8. - Theoretical and experimental stresses in test specimen (from ref. 10). Cassinian parameters m = 1.0 and n = 1.9; cylinder radius, 5.97 inches; wall thickness, 0.062 inch; internal pressure, 250 pounds per square inch; modulus of elasticity, 10^7 psi; Poisson's ratio, 0.333.

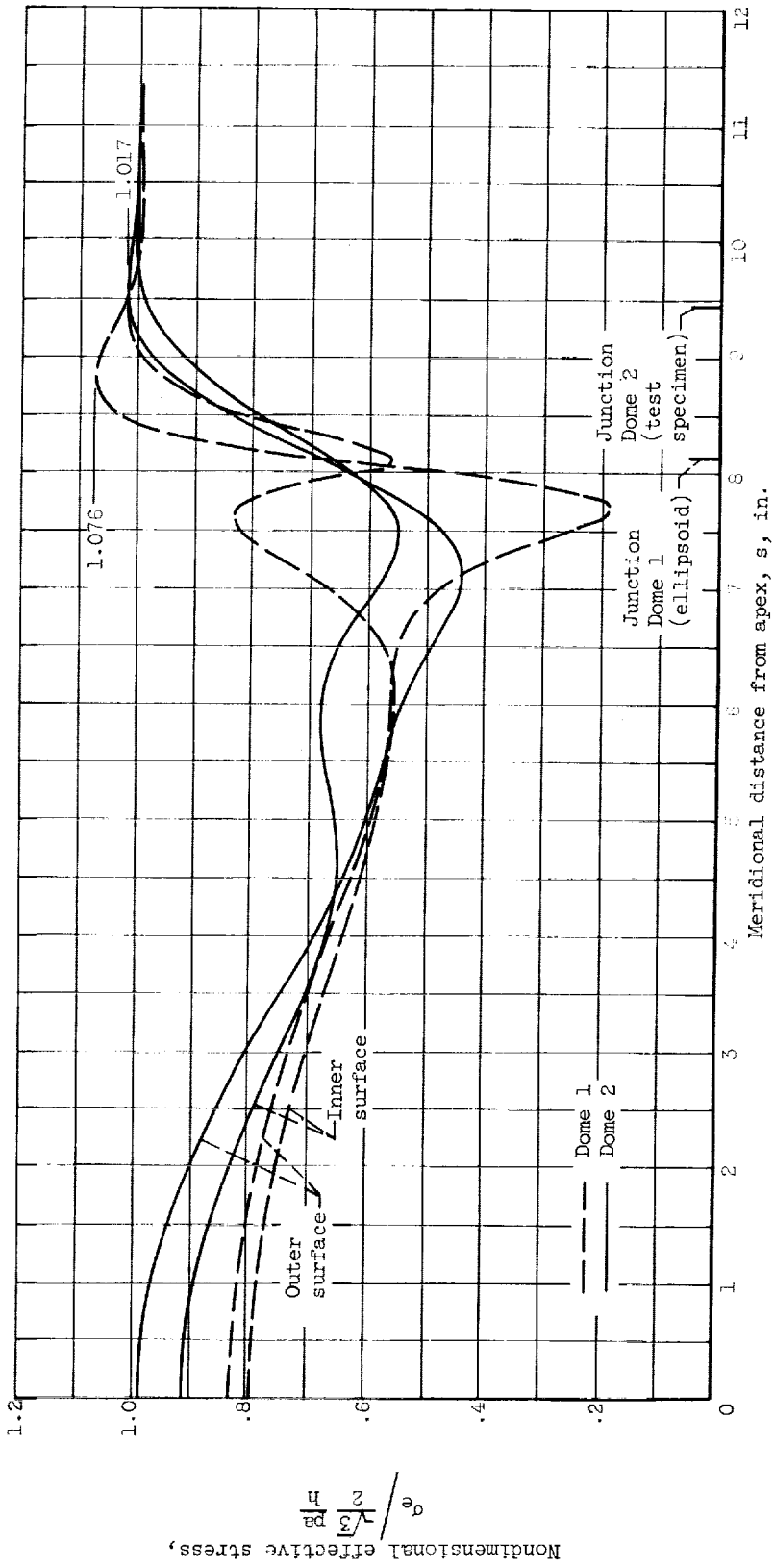

Figure 9. - Comparison of effective stresses in two Cassinian domes (from ref. 10). Cylinder radii, 5.97 inches; wall thicknesses, 0.062 inch; modulus of elasticity, 10^7 psi; Poisson's ratio, 0.333. Cassinian parameters, m = 0 and n = 1.414 for dome 1; m = 1.000 and n = 1.900 for dome 2.